Supplementary Information (SI) for Journal of Materials Chemistry A.
This journal is © The Royal Society of Chemistry 2026

Supporting Information

Mechanochemically Engineered Defect-Rich Zn/Co–ZIF-8 Solid Solutions for Enhanced Electrochemical Water Splitting

(Supporting Information: 39 pages including this page)

Priyanka Kumari,[b†] Abdul Kareem,[b†] Mebin Varghese,[b] Arjun Warrier,[b] Sellappen Senthilkumar,[b] Tamas Panda[a]*

[a] *Centre for Clean Environment (CCE), Vellore Institute of Technology, Vellore Campus, Vellore-, 632014, Tamil Nadu, India.*

[b]*Department of Chemistry, School of Advanced Science, Vellore Institute of Technology, Vellore- 632014, Tamil Nadu, India.*

E-mail: tamaskumarpanda@vit.ac.in.

CONTENT

.

S1 (Section): Experimental measurements and methods:

General Remarks: Methanol (MeOH), 2-methylimidazole, Zinc nitrate hexahydrate, Cobalt nitrate hexahydrate, were purchased from Avra chemicals. All the chemicals and solvents were used without further purification. Solvothermal Experiment were performed in 5 mL culture tube inside a programmed oven for the synthesis of *p*Zn-ZIF-8-HT and *p*Co-ZIF-8-HT.

Ball mill, TGA, FT-IR, Raman Spectra, PXRD, N_2 gas adsorption, XPS, UV-Visible Spectrophotometer, AAS, FE-SEM, HR-TEM measurement, STEM and ICP-MS: FRITSCH GmbH milling and Sizing Industriestrasse 8, Germany (grinding bowl 45 ml hardened, stainless steel- grinding ball 10 mm hardened, seal ring PTFE). TGA (Thermo-gravimetric Analysis) was carried out on Model: SDTQ600) Make: TA Instruments, USA at a temperature range between 25 ^{o}C to 800 ^{o}C under N_2 atmosphere at a heating rate of 10^{o}Cmin^{-1}. The (Fourier transform) FT- IR spectrophotometer was taken on a Model: IR Affinity-I (Make: SHIMADZU Japan) with ATR attachment (Model: Specac). The Raman Spectra was taken on a Model: Cora 5001 DUAL (Maker: Anton Paar). PXRD (Powder X-ray diffraction) analysis were performed using Bruker DS advance instrument using iron-filtered Cu Kα radiation (λ=1.5406 Å) in the 2θ range of 5°-50° with a step size of 0.02° and a time of 0.3 seconds per step. The N_2 gas adsorption was taken on a Model: Quantachrome USA (Maker: AutosorbiQ). X-ray Photoelectron Spectroscopy (XPS) with Auger Electron Spectroscopy(AES) Module Model/Supplier:PHI 5000 Versa Prob II, FEI Inc. UV-Visible Spectrophotometer-JASCO (V-670 PC). The AAS was taken on a Model: AANALYST 400 (Maker: Perkin Elmer). FE-SEM (Field Emission Scanning Electron Microscopy) analysis were performed on CARL ZEISS with energy dispersive spectroscopy (EDS) from oxford instruments, 300 n microtensile stage from gatan and sputter coating set-up. The HR-TEM images was taken on a Model: G2-20 TWIN (Operating voltage 200 kV) (Maker: FEI-TECNAI). STEM was taken on Model: Themis 300 G3. ICP-MS was taken on a Model: ICS 6000 Ion Chromatography System, iCAP RQ ICP-MS.

Section S2. Detailed synthetic procedures and PXRD patterns for *p*Zn-ZIF-8-RT/HT, *p*Co-ZIF-8-RT/HT, *a*-$Zn_{50}Co_{50}$ZIF8-RT/HT and *c*-$Zn_{50}Co_{50}$ZIF8-RT/HT.

Synthesis of *p*Zn-ZIF-8-RT and *p*Co-ZIF-8-RT: We followed the synthesis procedure of ***p*Zn-**ZIF-8-HT and *p*Co-ZIF-8-HT from the reported literature.[1a]

Synthesis of *p*Zn-ZIF-8-HT and *p*Co-ZIF-8-HT: We followed the synthesis procedure of ***p*Zn-**ZIF-8-HT and *p*Co-ZIF-8-HT from the published literature.[1b]

Synthesis of amorphous solid solution (*a*-$Zn_{50}Co_{50}$ZIF8-RT): Degassed *p*Zn-ZIF-8-RT (0.5 mmol, 0.186 g) and *p*Co-ZIF-8-RT (0.5 mmol, 0.183 g) were kept in 10 mL stainless steel jar containing 10 balls inside (7mm diameter) under Ar atmosphere. The ball mill reaction was performed in Fritsch, Pulverisette 7 instrument with rotation speed of 400 rpm for 2 h including 5 minutes grinding and 5 minutes pause under Ar atmosphere. As-synthesized amorphous solid solution product was obtained by scratching the wall of the stainless-steel jar.

Synthesis of crystalline solid solution (*c*-$Zn_{50}Co_{50}$ZIF8-RT): 0.5 g of *a*-$Zn_{50}Co_{50}$ZIF-8 was kept at 25 °C in 95% RH for 3 days. Further, the sample was degassed at 100 °C for 12 h. The final product named as *c*-$Zn_{50}Co_{50}$ZIF8-RT.

Synthesis of amorphous solid solution (*a*-$Zn_{50}Co_{50}$ZIF8-HT): Synthesis of *a*-$Zn_{50}Co_{50}$ZIF8-HT followed in the similar synthesis procedure of *a*-$Zn_{50}Co_{50}$ZIF8-RT except we used degassed *p*Zn-ZIF-8-HT and *p*Co-ZIF-8-HT instead of *p*Zn-ZIF-8-RT and *p*Co-ZIF-8-RT.

Synthesis of crystalline solid solution (*c*-$Zn_{50}Co_{50}$ZIF8-HT): 0.5 g of *a*-$Zn_{50}Co_{50}$ZIF8-HT was kept at 25 °C in 95% RH in a humidity chember for 3 days. Further, the sample was degassed at 100 °C for 12 h. The final product named as *c*-$Zn_{50}Co_{50}$ZIF8-HT.

Experimental PXRD Pattern of *p*Zn-ZIF-8-RT/HT, *p*Co-ZIF-8-RT/HT, *a*-$Zn_{50}Co_{50}$ZIF8-RT/HT and *c*-$Zn_{50}Co_{50}$ZIF8-RT/HT:

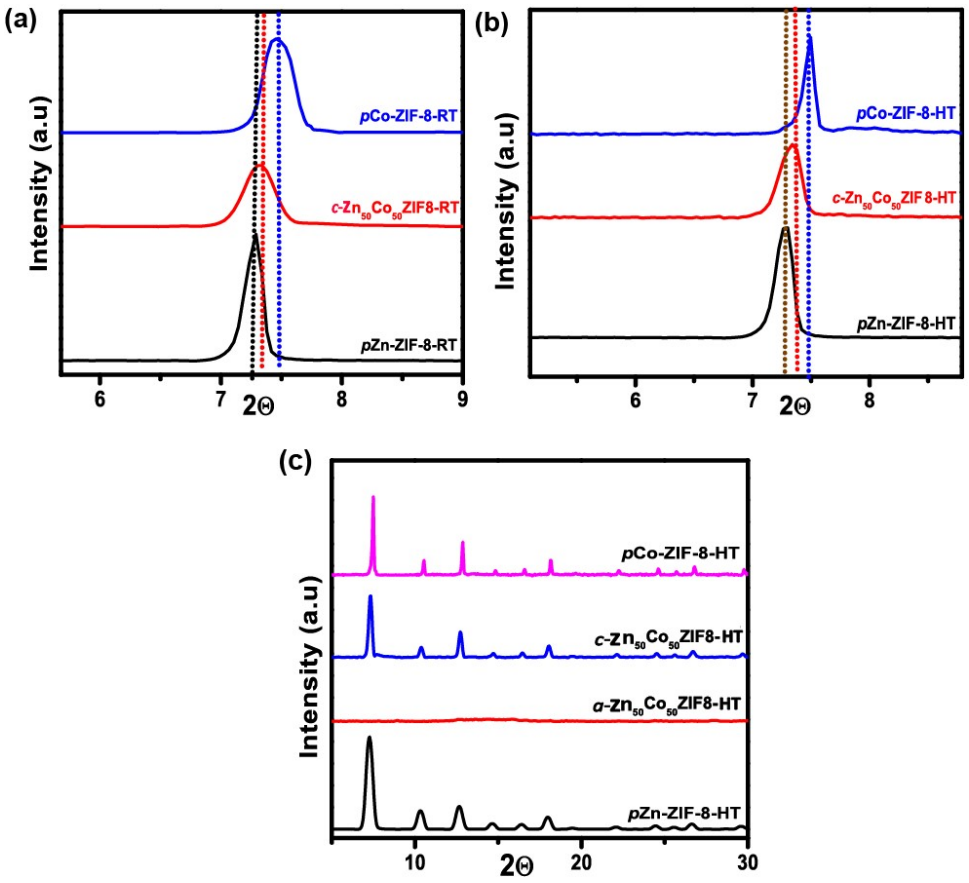

Figure S1. Experimental PXRD pattern of (a) room temperature synthesis of *c*-$Zn_{50}Co_{50}$ZIF8-RT in comparison with *p*Zn-ZIF-8-RT and *p*Co-ZIF-8-RT at different 2Θ range, (b) solvothermally synthesized *c*-$Zn_{50}Co_{50}$ZIF8-HT in comparison with *p*Zn-ZIF-8-HT and *p*Co-ZIF-8-HT at different 2Θ range, (c) solvothermally synthesized *p*Zn-ZIF-8-HT (black), *a*-$Zn_{50}Co_{50}$ZIF-8-HT (red), *c*-$Zn_{50}Co_{50}$ZIF8-HT (blue), *p*Co-ZIF-8-HT (pink) crystals.

Section S3: N_2 gas adsorption isotherm, t-plot, BJH pore size distribution, TGA, FT-IR, FE-SEM images and HR-TEM images.

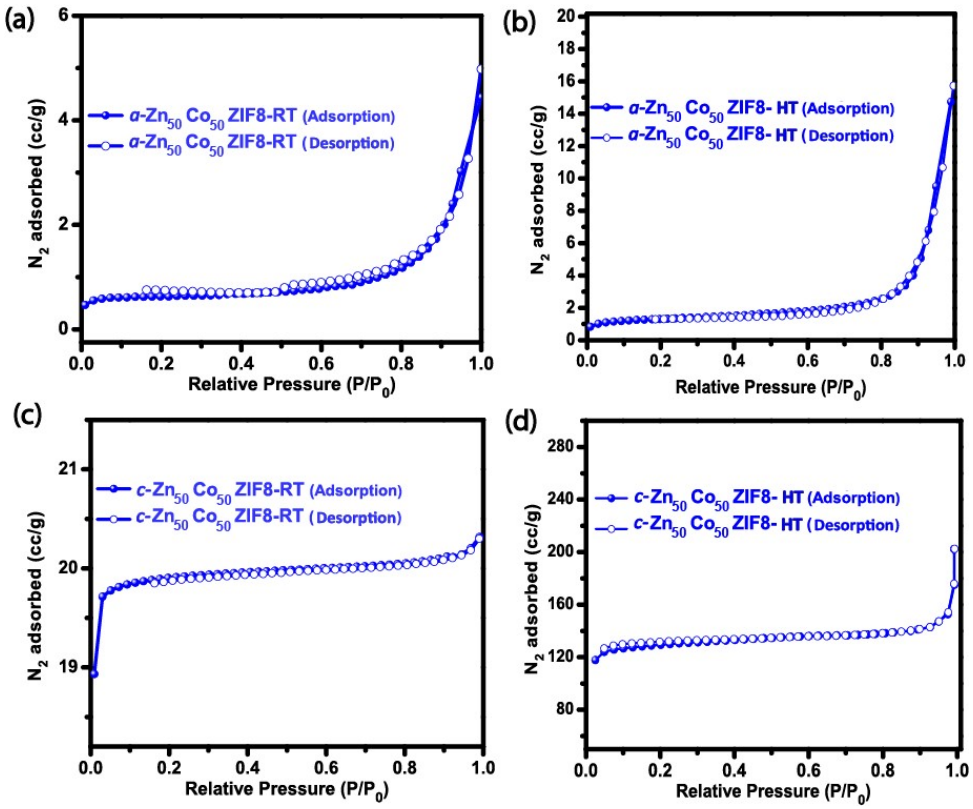

Figure S2: N_2 gas adsorption isotherm of (a) *a*-$Zn_{50}Co_{50}$ZIF8-RT, (b) *a*-$Zn_{50}Co_{50}$ZIF8-HT, (c) *c*-$Zn_{50}Co_{50}$ZIF8-RT, (d) *c*-$Zn_{50}Co_{50}$ZIF8-HT, respectively.

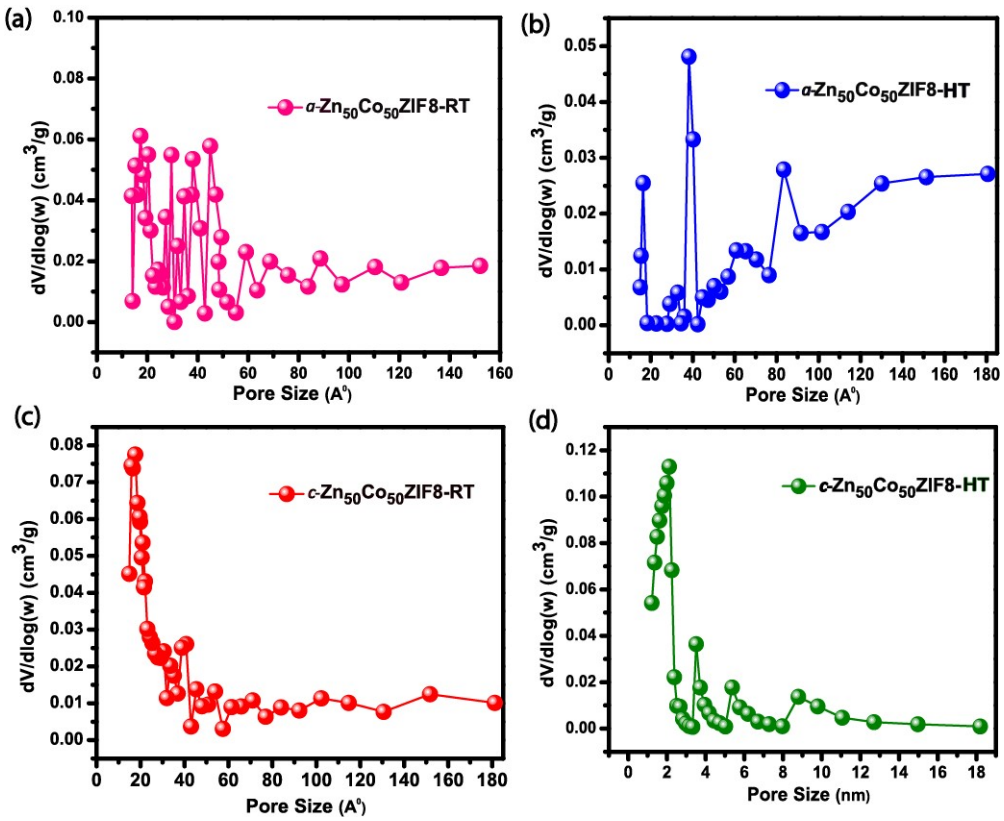

Figure S3: The BJH pore size distribution of (a) *a*-$Zn_{50}Co_{50}$ZIF8-RT, (b) *a*-$Zn_{50}Co_{50}$ZIF8-HT, (c) *c*-$Zn_{50}Co_{50}$ZIF8-RT, and (d) *c*-$Zn_{50}Co_{50}$ZIF8-HT, measured from the nitrogen sorption isotherm data.

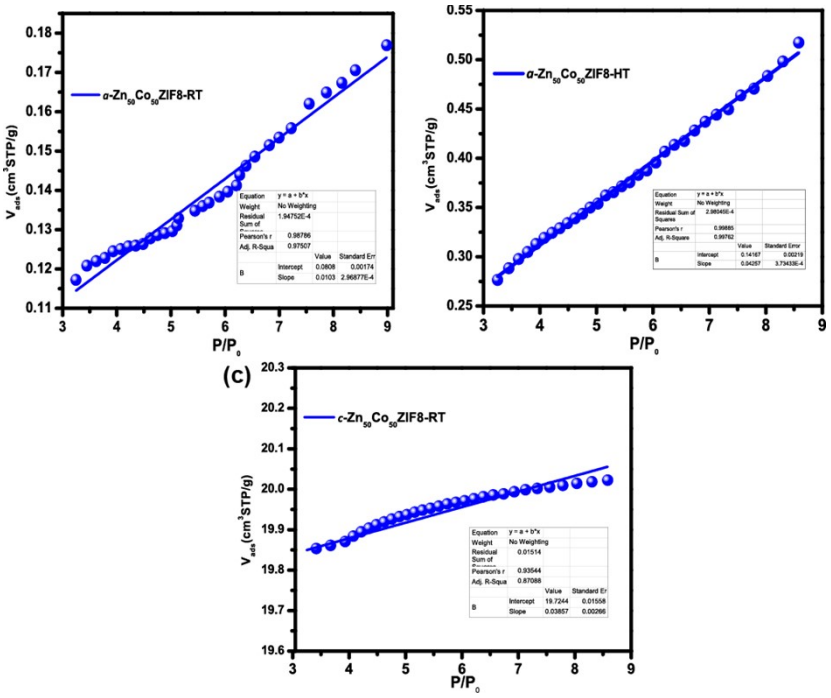

Figure S4: t-plot of (a) *a*-$Zn_{50}Co_{50}$ZIF8-RT, (b) *c*-$Zn_{50}Co_{50}$ZIF8-RT, and (c) *a*-$Zn_{50}Co_{50}$ZIF8-HT, respectively.

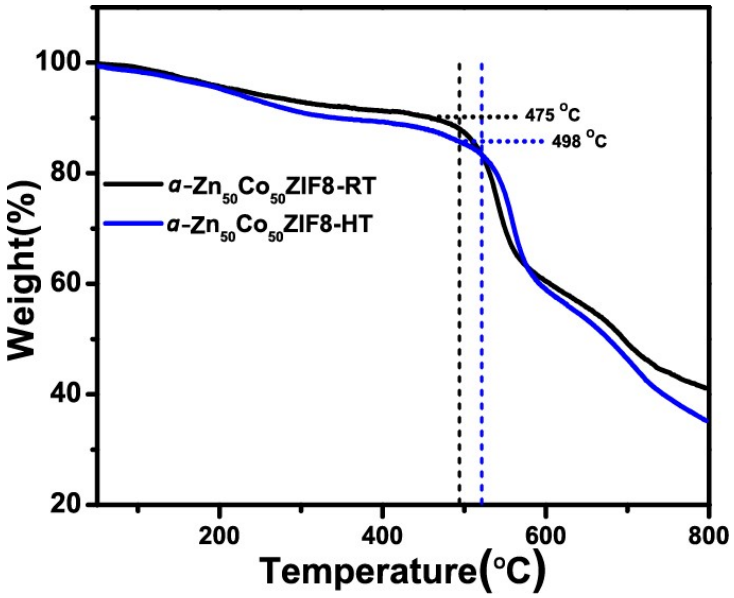

Figure S5: Thermogravimetric analysis (TGA) for the as-synthesized *a*-$Zn_{50}Co_{50}$ZIF8-RT, and (b) *a*-$Zn_{50}Co_{50}$ZIF8-HT.

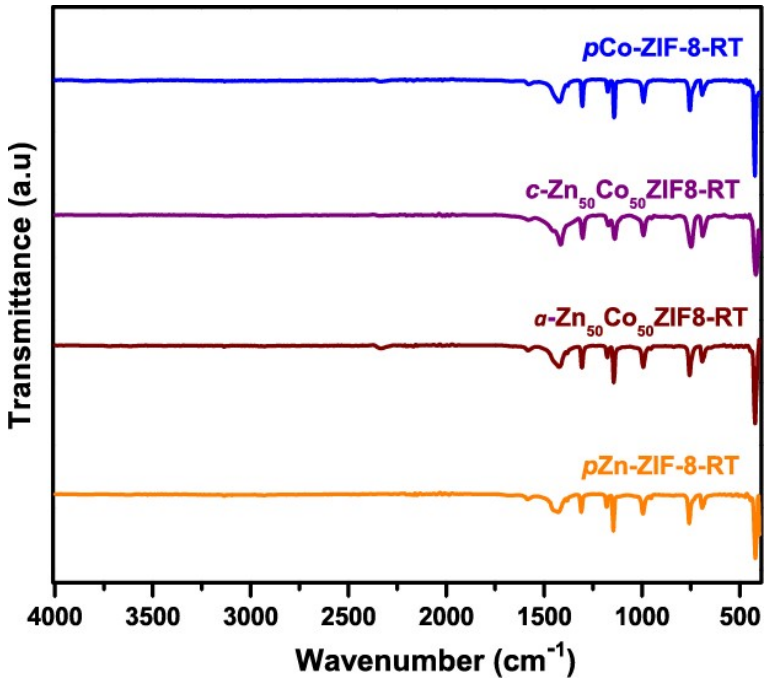

Figure S6: FT-IR of (a) *p*Zn-ZIF-8-RT (yellow), (b) *a*-$Zn_{50}Co_{50}$ZIF8-RT (brown), (c) *c*-$Zn_{50}Co_{50}$ZIF8-RT (violet), (d) *p*Co-ZIF-8-RT (blue), respectively.

FE-SEM Images:

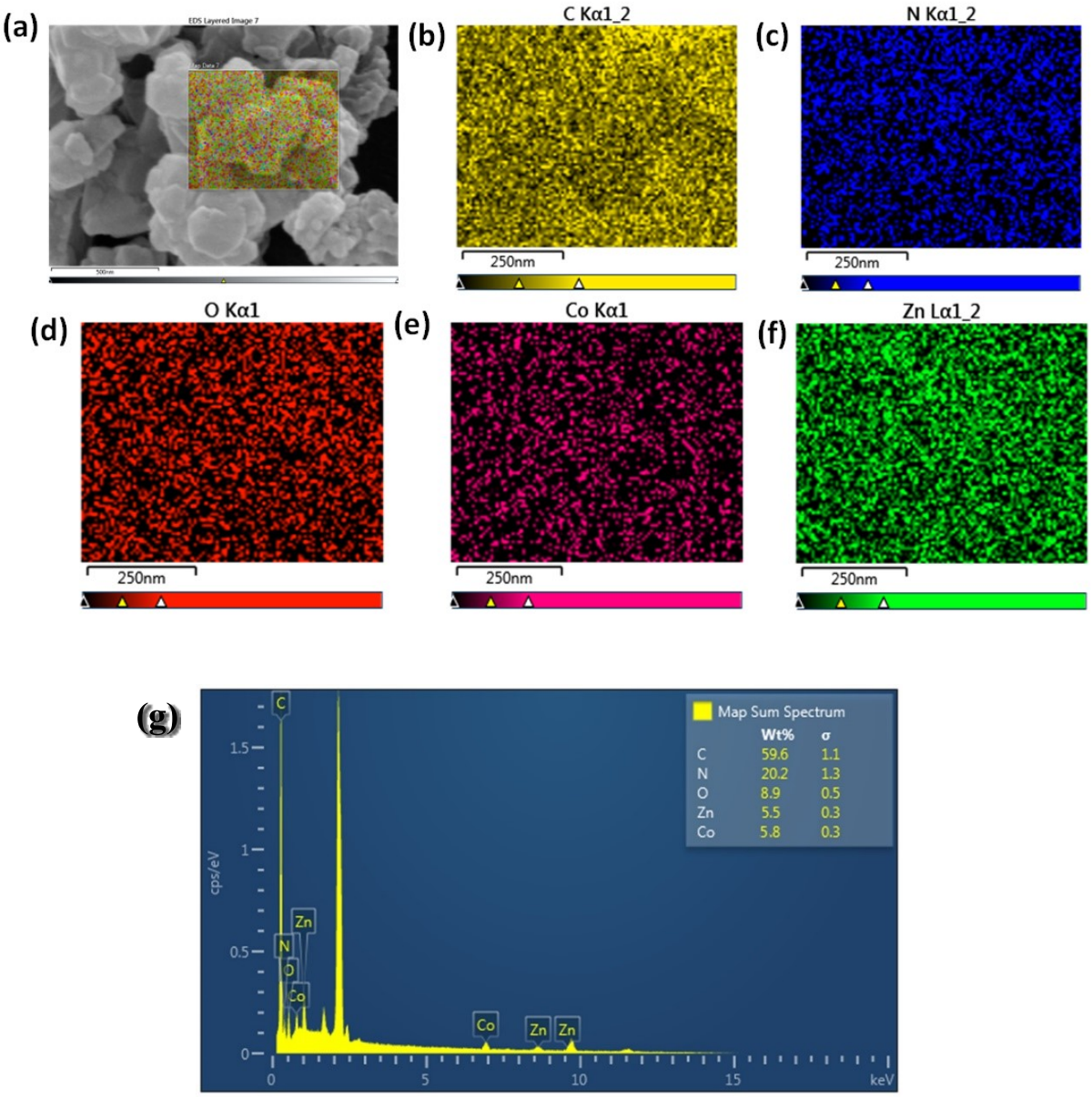

Figure S7: FE-SEM-EDAX elemental mapping of *a*-$Zn_{50}Co_{50}$ZIF8-RT (a) FE-SEM images of the particle selected for elemental mapping (b) C distribution (c) N distribution (d) O distribution (e) Co distribution (f) Zn distribution and (g) EDAX spectrum of elemental mapping.

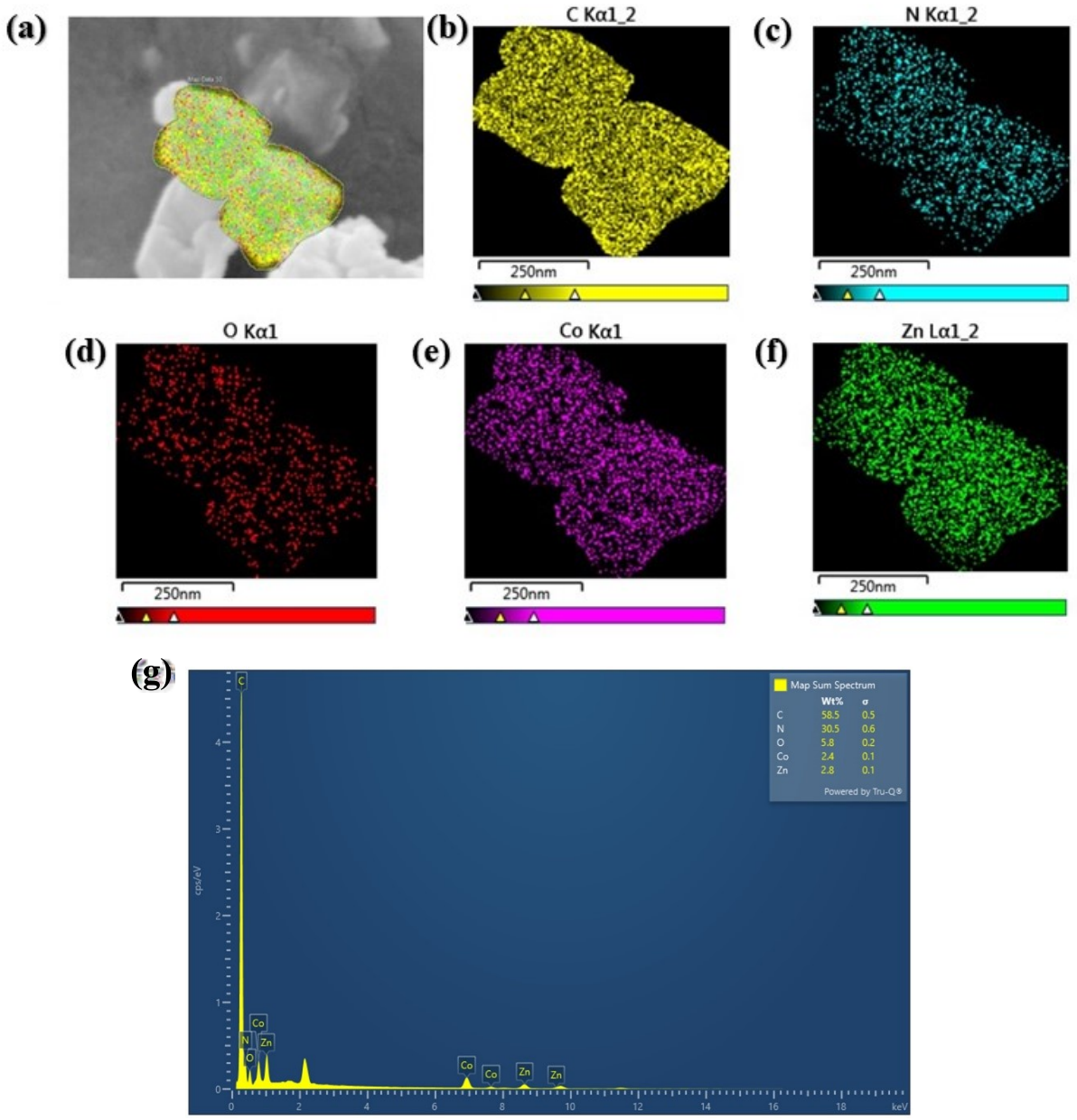

Figure S8: FE-SEM-EDAX elemental mapping of *c*-$Zn_{50}Co_{50}$ZIF8-RT (a) FE-SEM images of the particle selected for elemental mapping (b) C distribution (c) N distribution (d) O distribution (e) Co distribution (f) Zn distribution and (g) EDAX spectrum of elemental mapping.

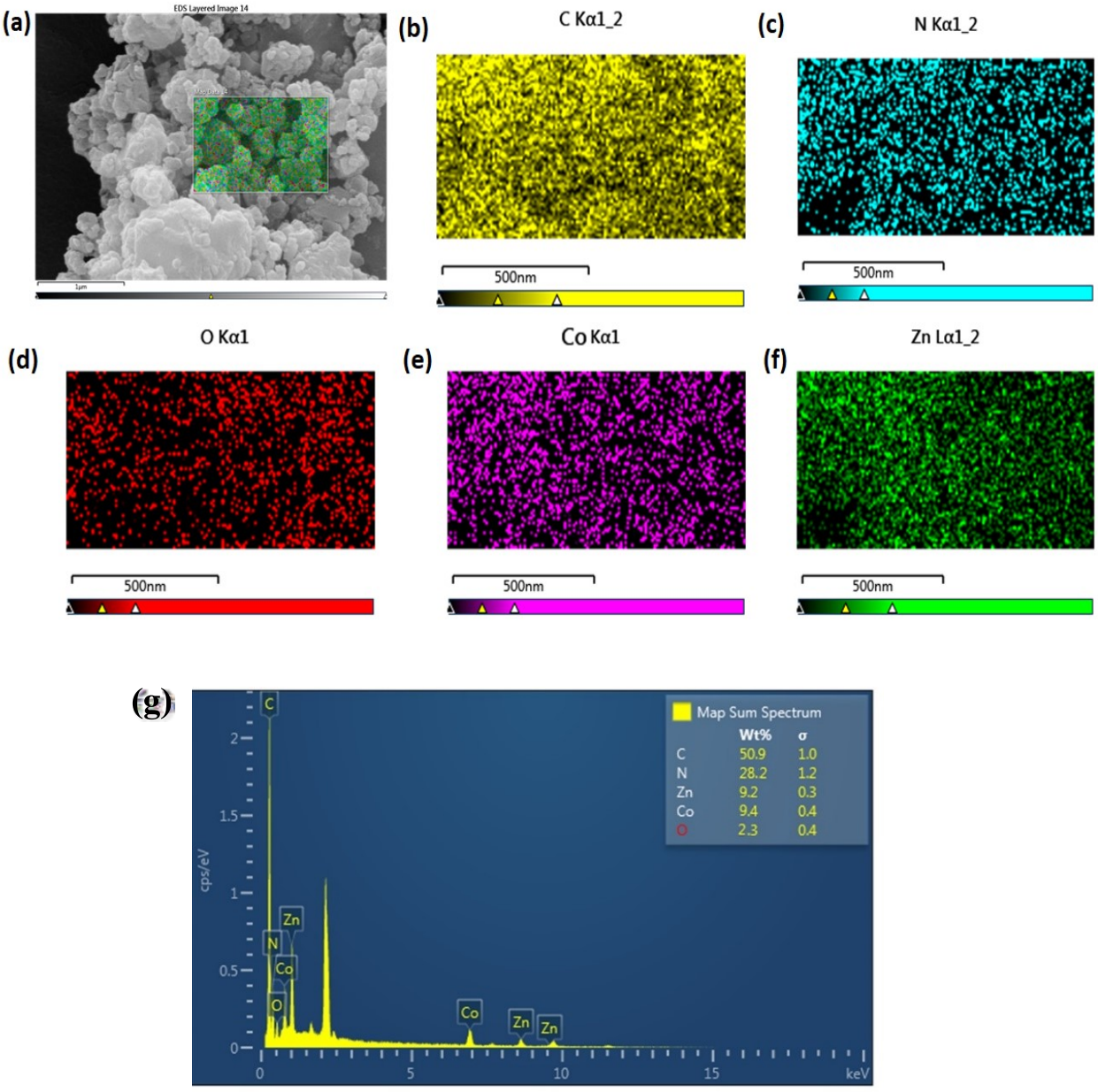

Figure S9: FE-SEM-EDAX elemental mapping of *a*-$Zn_{50}Co_{50}$ZIF8-HT (1:1 mixture of *p*Zn-ZIF-8-HT and *p*Co-ZIF-8-HT) (a) FE-SEM images of the particle selected for elemental mapping (b) C distribution (c) N distribution (d) O distribution (e) Co distribution (f) Zn distribution and (g) EDAX spectrum of elemental mapping.

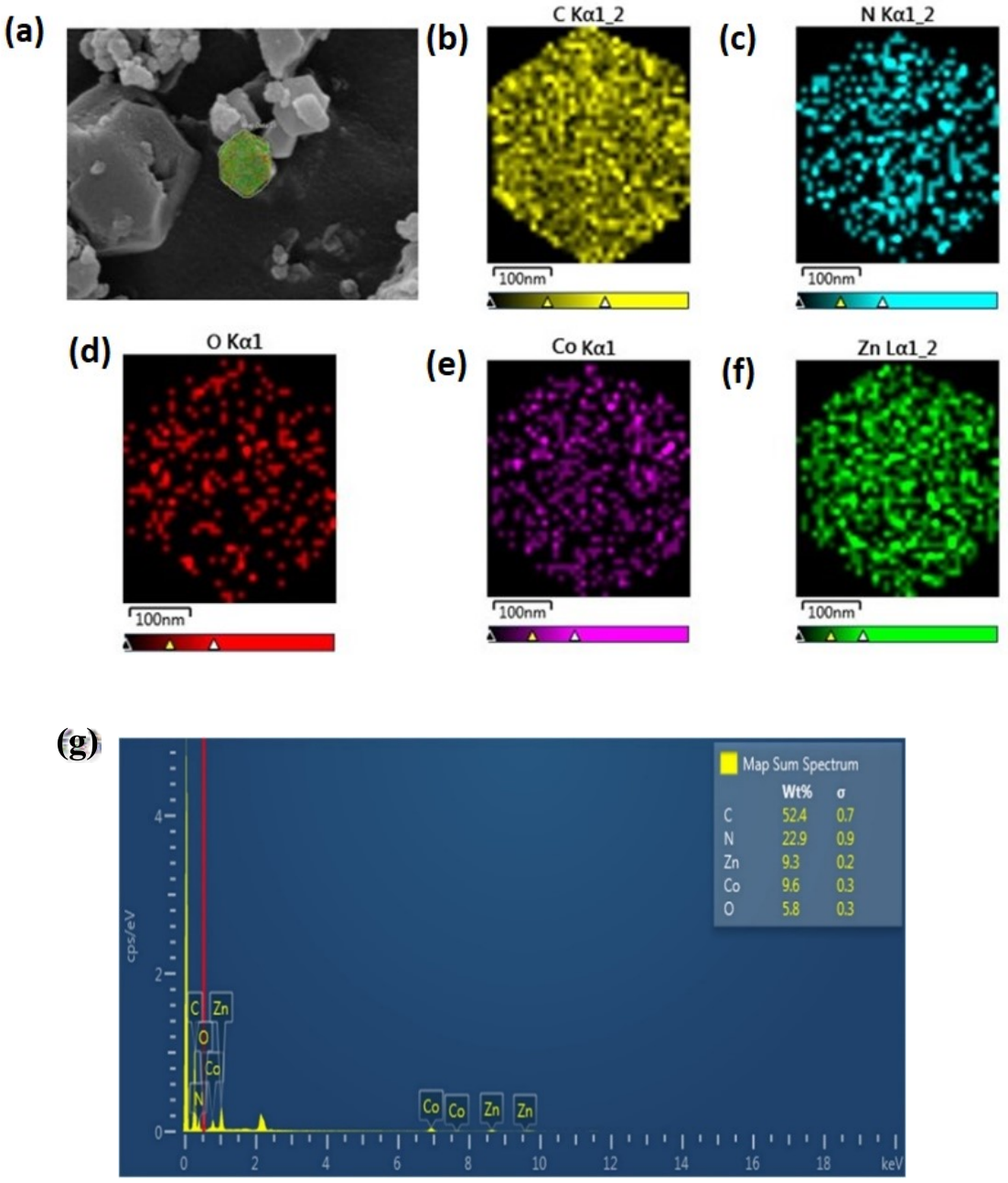

Figure S10: FE-SEM-EDAX elemental mapping of *c*-$Zn_{50}Co_{50}$ZIF8-HT (a) FE-SEM images of the particle selected for elemental mapping (b) C distribution (c) N distribution (d) O distribution (e) Co distribution (f) Zn distribution and (g) EDAX spectrum of elemental mapping.

HR-TEM Images:

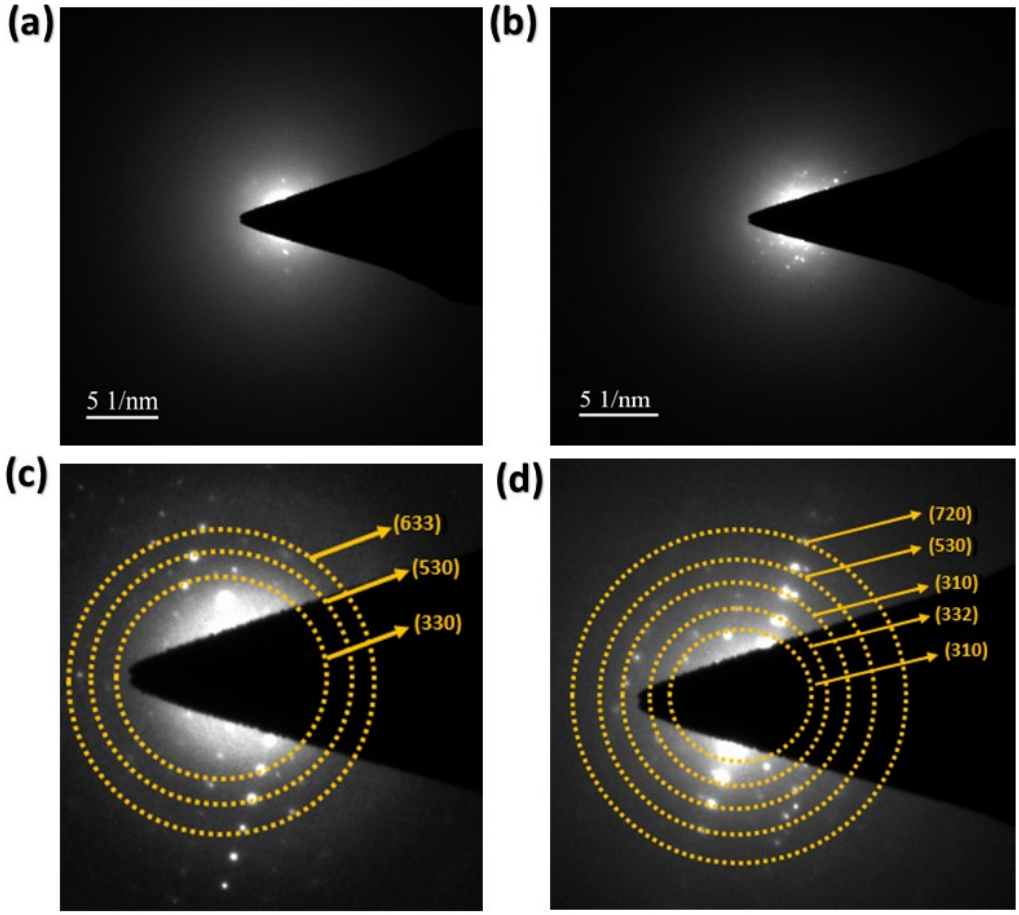

Figure S11: SAED Pattern of (a) *a*-$Zn_{50}Co_{50}$ZIF8-RT, (b) *a*-$Zn_{50}Co_{50}$ZIF8-HT, (c) *c*-$Zn_{50}Co_{50}$ZIF8-RT and (d) *c*-$Zn_{50}Co_{50}$ZIF8-HT, respectively.

S3.1: AAS (atomic absorption spectrometry) Analysis

AAS analysis were performed for *a*-$Zn_{50}Co_{50}$ZIF8-RT, *c*-$Zn_{50}Co_{50}$ZIF8-RT, *a*-$Zn_{50}Co_{50}$ZIF8-HT, *c*-$Zn_{50}Co_{50}$ZIF8-HT catalysts to determine the concentration of Zn and Co metal ion. The dry powder of different catalysts was dissove in 1M H_2SO_4 separately. Further, 5, 10 and 20 ppm solution of Zinc and Cobalt metal salt were prepared. The molar concentration of Zinc and Cobalt metal ion were measured and ratio of different catalysts were calculated.

Table S1: Atomic Absorption Spectroscopy (AAS) Data:

Sample No.	Zinc (mg/L)	Cobalt (mg/L)	Ratio
a-$Zn_{50}Co_{50}$ZIF8-RT	44	45	1:1
c-$Zn_{50}Co_{50}$ZIF8-RT	46	47	1:1
a-$Zn_{50}Co_{50}$ZIF8-HT	48	49	1:1
c-$Zn_{50}Co_{50}$ZIF8-HT	47	48	1:1

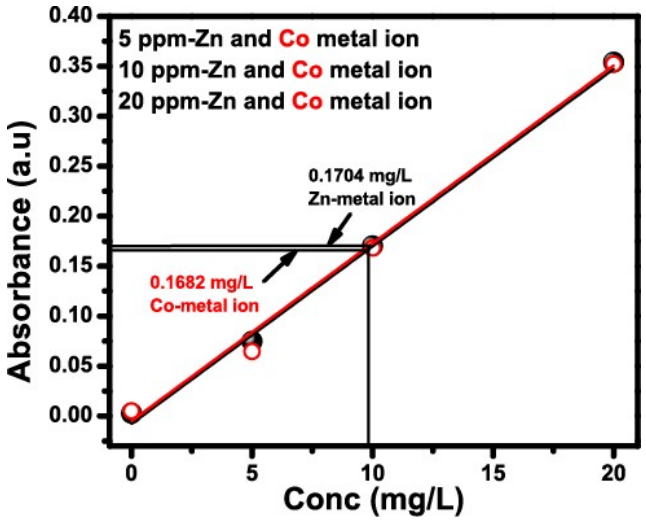

Figure S12: Atomic absorption spectrometry (AAS) analysis of (a, b) Zinc (black) and Cobalt (red) metal ions at 5, 10 and 20 ppm, (c) *a*-$Zn_{50}Co_{50}$ZIF8-RT (Zn-black, Co-red), *a*-$Zn_{50}Co_{50}$ZIF8-HT (Zn-blue, Co-pink), *c*-$Zn_{50}Co_{50}$ZIF8-RT (Zn-green, Co-dark blue) and *c*-$Zn_{50}Co_{50}$ZIF8-HT (Zn-purple, Co-violet).

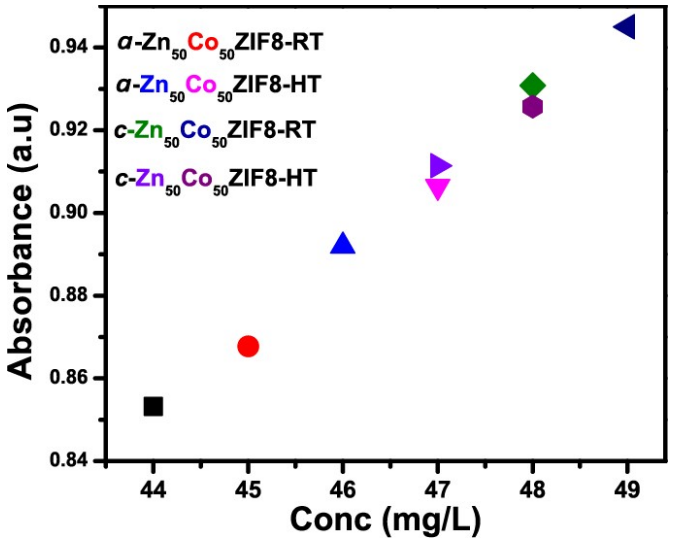

Figure S13: Atomic absorption spectrometry (AAS) analysis of (a, b) Zinc (black) and Cobalt (red) metal ions at 5, 10 and 20 ppm, (c) *a*-$Zn_{50}Co_{50}$ZIF8-RT (Zn-black, Co-red), *a*-$Zn_{50}Co_{50}$ZIF8-HT (Zn-blue, Co-pink), *c*-$Zn_{50}Co_{50}$ZIF8-RT (Zn-green, Co-dark blue) and *c*-$Zn_{50}Co_{50}$ZIF8-HT (Zn-purple, Co-violet).

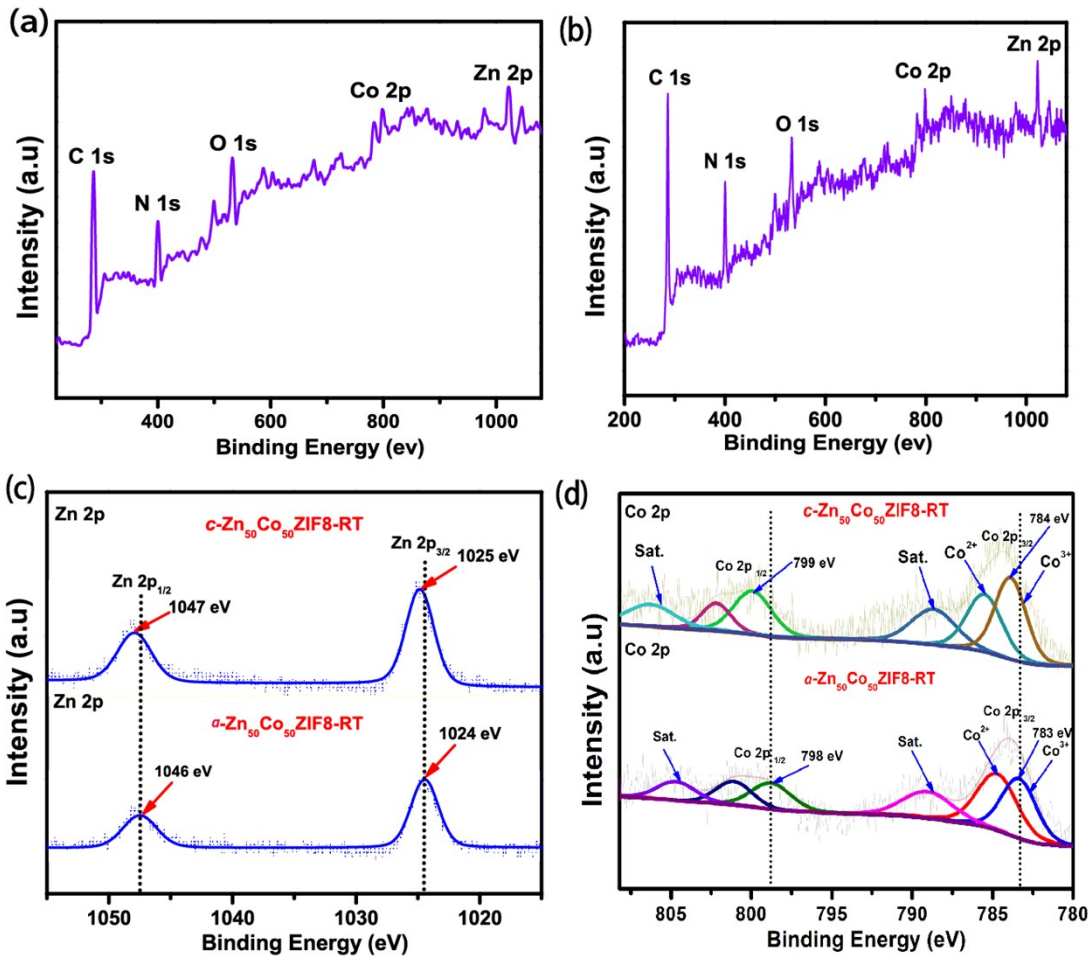

Figure S14: XPS (a, b) detailed line scans of the *a*-$Zn_{50}Co_{50}$ZIF8-RT and *c*-$Zn_{50}Co_{50}$ZIF8-RT, (c) Zn 2p peak of *a*-$Zn_{50}Co_{50}$ZIF8-RT and *c*-$Zn_{50}Co_{50}$ZIF8-RT, (d) Co 2p peak of *a*-$Zn_{50}Co_{50}$ZIF8-RT and *c*-$Zn_{50}Co_{50}$ZIF8-RT.

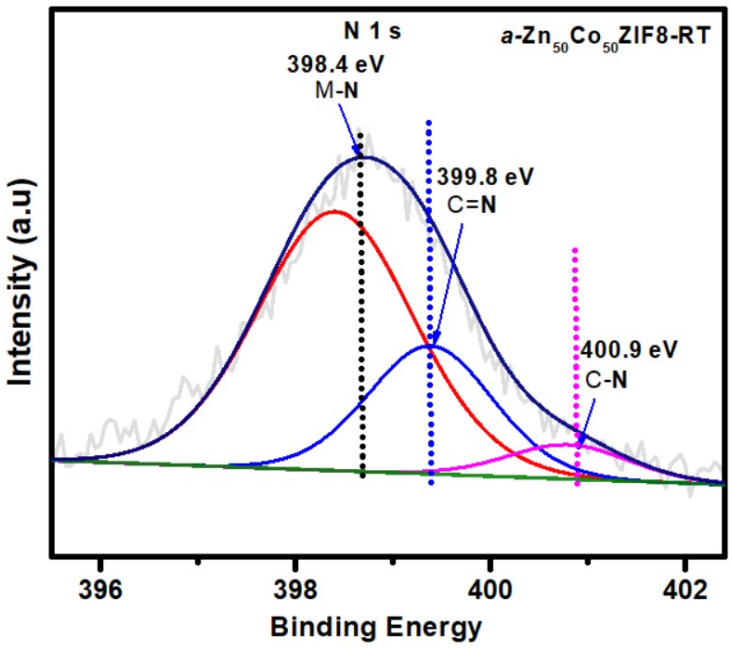

Figure S15: N 1s spectra of *a*-$Zn_{50}Co_{50}$ZIF8-RT.

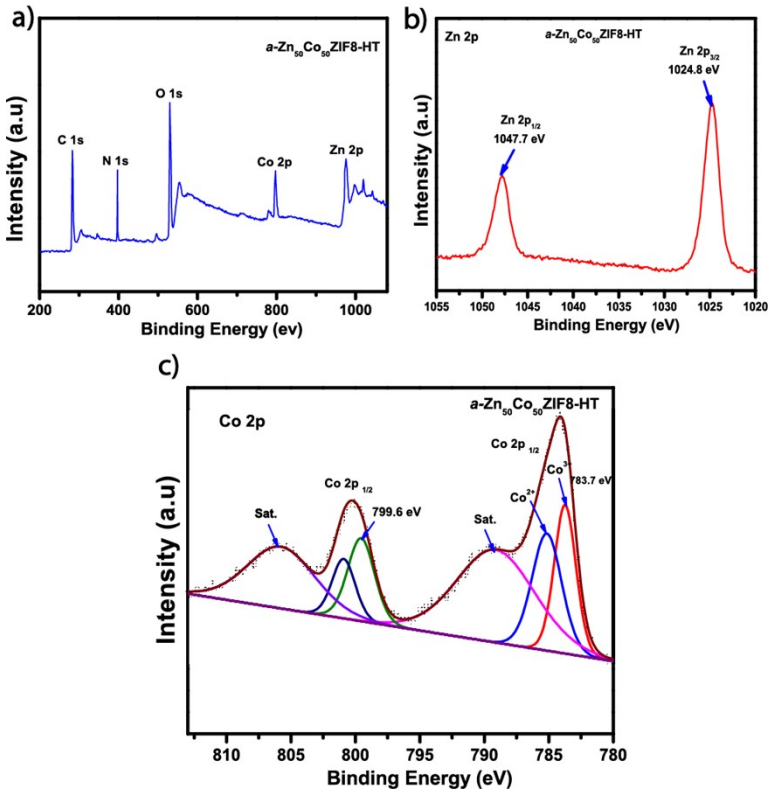

Figure S16: XPS (a) detailed line scans of the *a*-$Zn_{50}Co_{50}$ZIF8-HT (b) Zn 2p peak of *a*-$Zn_{50}Co_{50}$ZIF8-HT and, (C) Co 2p peak of *a*-$Zn_{50}Co_{50}$ZIF8-HT.

S3.2 Stability Test:

Stability test in water and different solvents:

Stability of these solid solution materials were measured by using PXRD and FT-IR analysis. It is evident from the PXRD pattern that, *p*Zn-ZIF-8-RT and *c*-$Zn_{50}Co_{50}$ZIF8-RT are very much stable upto 14 days in water, while *p*Co-ZIF-8-RT crystal structure get collapse at 14 days in water at 25 °C (Figure S17a-c). In addition, *p*Co-ZIF-8-RT was found to be unstable at 70 °C after 2 days in water, as it is evident from their loss of low angle reflection and amorphous nature of PXRD pattern (FigureS17b). However, for *p*Zn-ZIF-8-RT exhibits high stability at 70 °C after 2 days in water confirmed by PXRD. Similarly, for *c*-$Zn_{50}Co_{50}$ZIF8-RT, all the peaks are retained with low intensity which shows that crystallinity of *c*-$Zn_{50}Co_{50}$ZIF8-RT has reduced at 70 °C in water (Figure S17c). Further, we also measure the stability of *c*-$Zn_{50}Co_{50}$ZIF8-RT in different solvent such as DMF, DMSO, acetone, DMAc, THF and hexane at 25 °C for 3 and at 70 °C for 2 days. It is evident from the PXRD pattern that, *c*-$Zn_{50}Co_{50}$ZIF8-RT are very much stable for 3 days and at 70 °C for 2 days under different solvent conditions (Figure S18c and d). FT-IR of *a*-$Zn_{50}Co_{50}$ZIF8-RT was analysed in different solvent such as DMF, DMSO, acetone, DMAc, THF and hexane at 25 °C for 3 days and at 70 °C for 2 days. It is evident from the FT-IR plot that, *a*-$Zn_{50}Co_{50}$ZIF8-RT are very much stable for 3 days and at 70 °C for 2 days under different solvent conditions (Figure S18a and b).

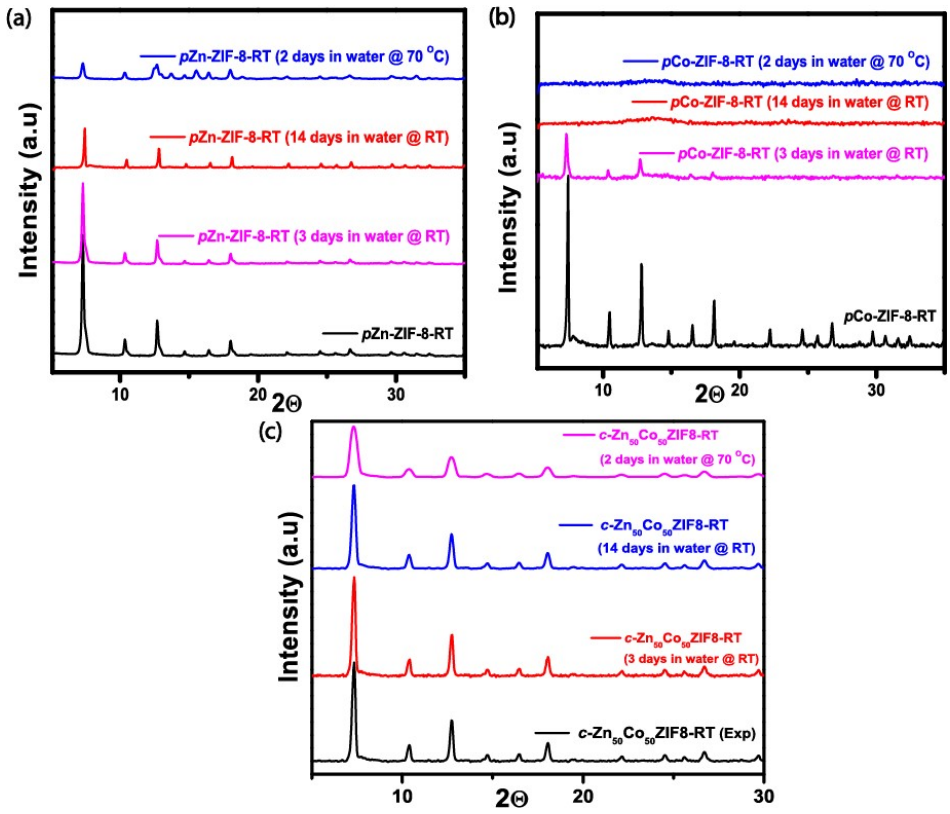

Figure S17*:* PXRD patterns of *p*Zn-ZIF-8-RT, (b) *p*Co-ZIF-8-RT and (c) *c*-$Zn_{50}Co_{50}$ZIF8-RT performed during the stability test in water (at 25 °C) for 3 days, 14 days and warm water (at 70 °C) for 2 days. (d) PXRD patterns of different solvent stability test for *c*-$Zn_{50}Co_{50}$ZIF8-RT at 25 °C for 3 days.

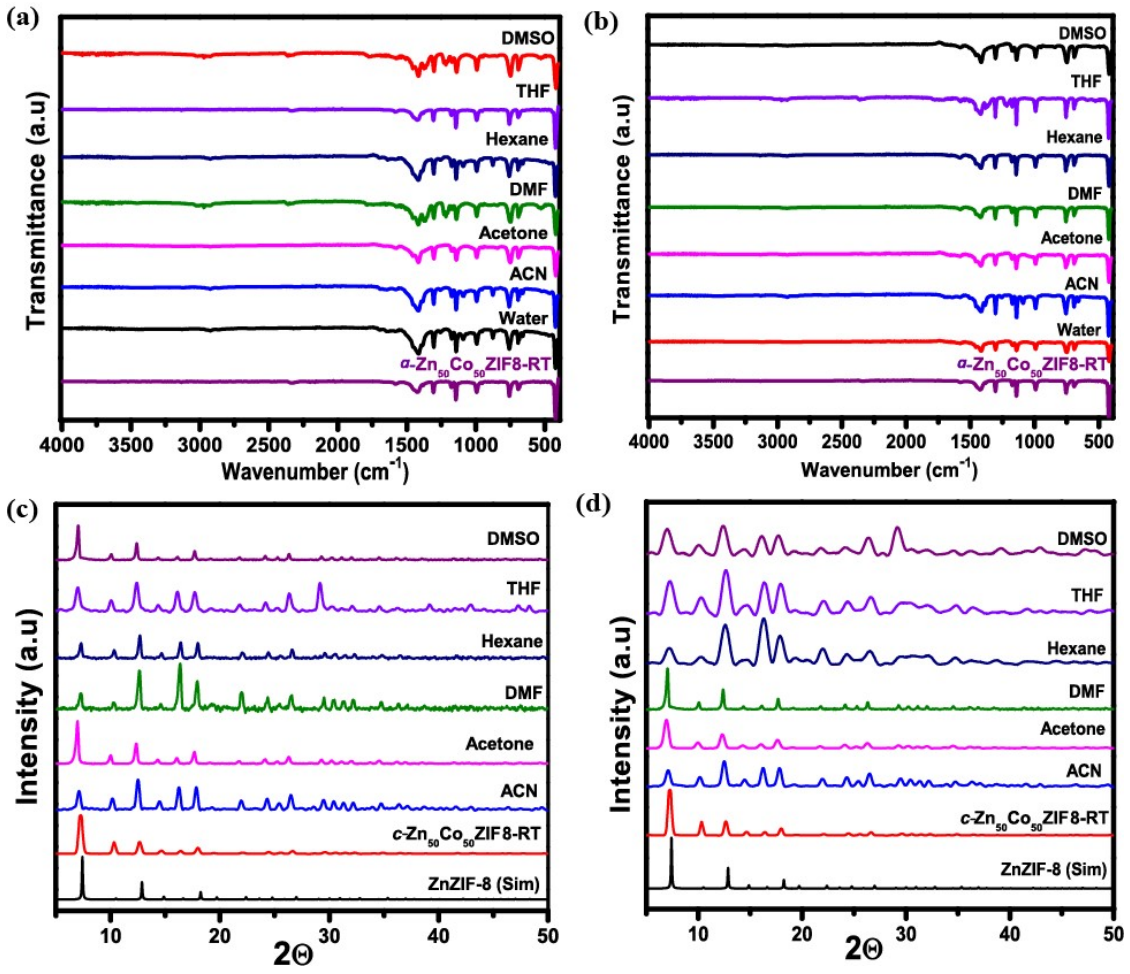

Figure S18*:* FT-IR spectra of (a) *a*-$Zn_{50}Co_{50}$ZIF8-RT performed during the different solvent stability test (at 25 °C) for 3 days, (b) *a*-$Zn_{50}Co_{50}$ZIF8-RT performed during the different solvent stability test (at 70 °C) for 2 days. PXRD patterns of different solvent stability test for *c*-$Zn_{50}Co_{50}$ZIF8-RT at (c) (at 25 °C) for 3 days, (d) 70 °C for 24 h.

Section 4: DFT study:

All DFT were conducted using Biovia Material Studio. We constructed a layer of ZIFs utilising the primary building unit. All structures were optimised using the B3LYP approach with a double numeric quality and a polarised functions (DNP) basis set. We calculated the highest occupied molecular orbital (HOMO) and lowest unoccupied molecular orbital (LUMO) energies for each molecule and subsequently plotted their energy band gaps. We also simulated a molecular electrostatic potential map (MESP) of all the optimized structures.

Red shaded region indicates more electronegative region, while blue shaded region denotes more electropositive region. The remaining colours correspond to the specified legend. It is clear from the MESP plot that, *a*-$Zn_{50}Co_{50}$ZIF8-RT have more red shaded region while *c*-$Zn_{50}Co_{50}$ZIF8-RT exhibit more green shaded region which indicate that *a*-$Zn_{50}Co_{50}$ZIF8-RT have more electron density available for transferring of electrons from valence band to conduction band compared to *c*-$Zn_{50}Co_{50}$ZIF8-RT and *p*Zn-ZIF-8-RT and *p*Co-ZIF-8-RT. MESP plot of *p*Zn-ZIF-8-RT and *p*Co-ZIF-8-RT shows more greenish blue shaded region and smaller greenish shaded region which indicate that both exhibit less electron density compared to *c*-$Zn_{50}Co_{50}$ZIF8-RT and *a*-$Zn_{50}Co_{50}$ZIF8-RT.

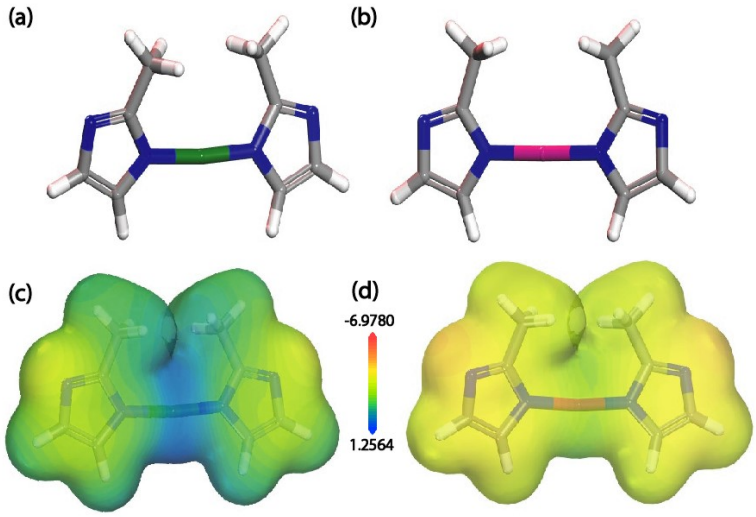

Figure S19: Optimized structure of pristine state of (a) *p*Zn-ZIF-8-RT, (b) *p*Co-ZIF-8-RT. Molecular electrostatic potential mapping (MESP) of (c, d) *p*Zn-ZIF-8-RT and *p*Co-ZIF-8-RT.

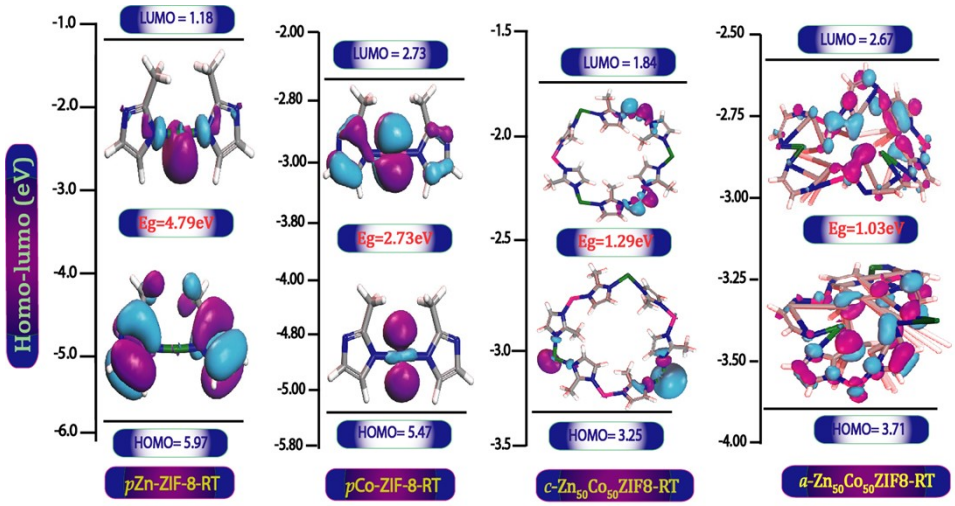

Figure S20: DFT calculation results of charge density distribution and band gap.

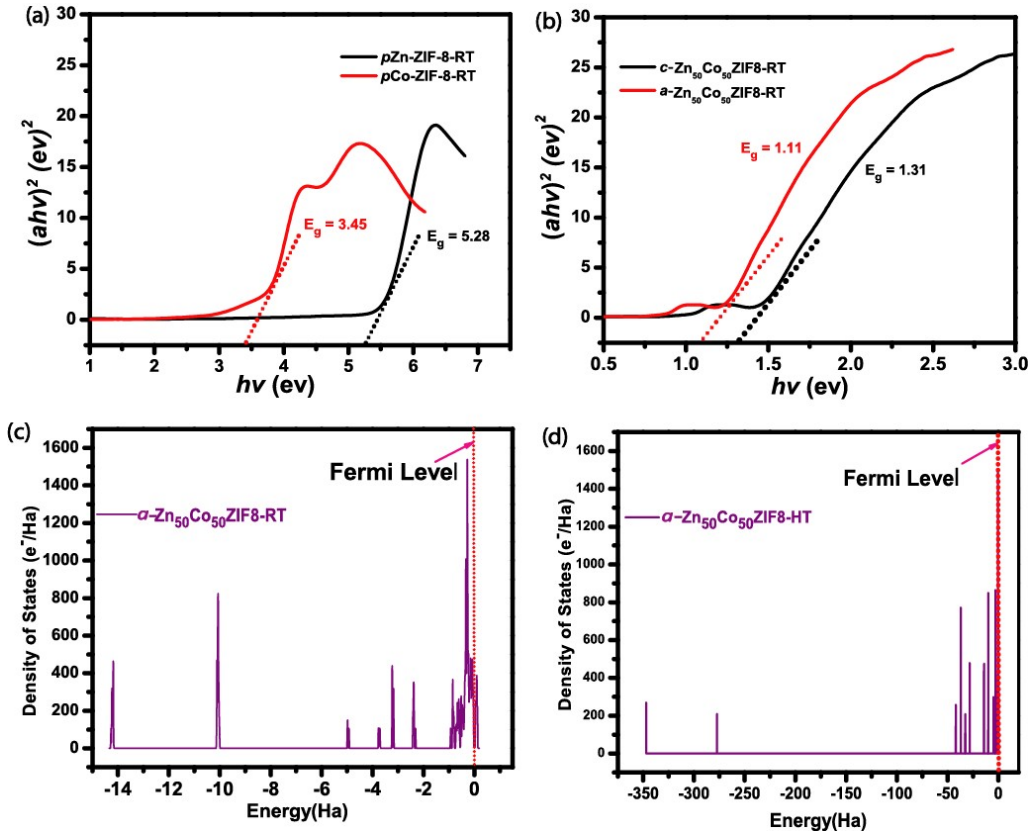

Figure S21: Optical band gap of (a) *p*Zn-ZIF-8-RT, *p*Co-ZIF-8-RT, (b) *a*-$Zn_{50}Co_{50}$ZIF8-RT and *c*-$Zn_{50}Co_{50}$ZIF8-RT. (c, d) Density of states of *a*-$Zn_{50}Co_{50}$ZIF8-RT and *c*-$Zn_{50}Co_{50}$ZIF8-RT.

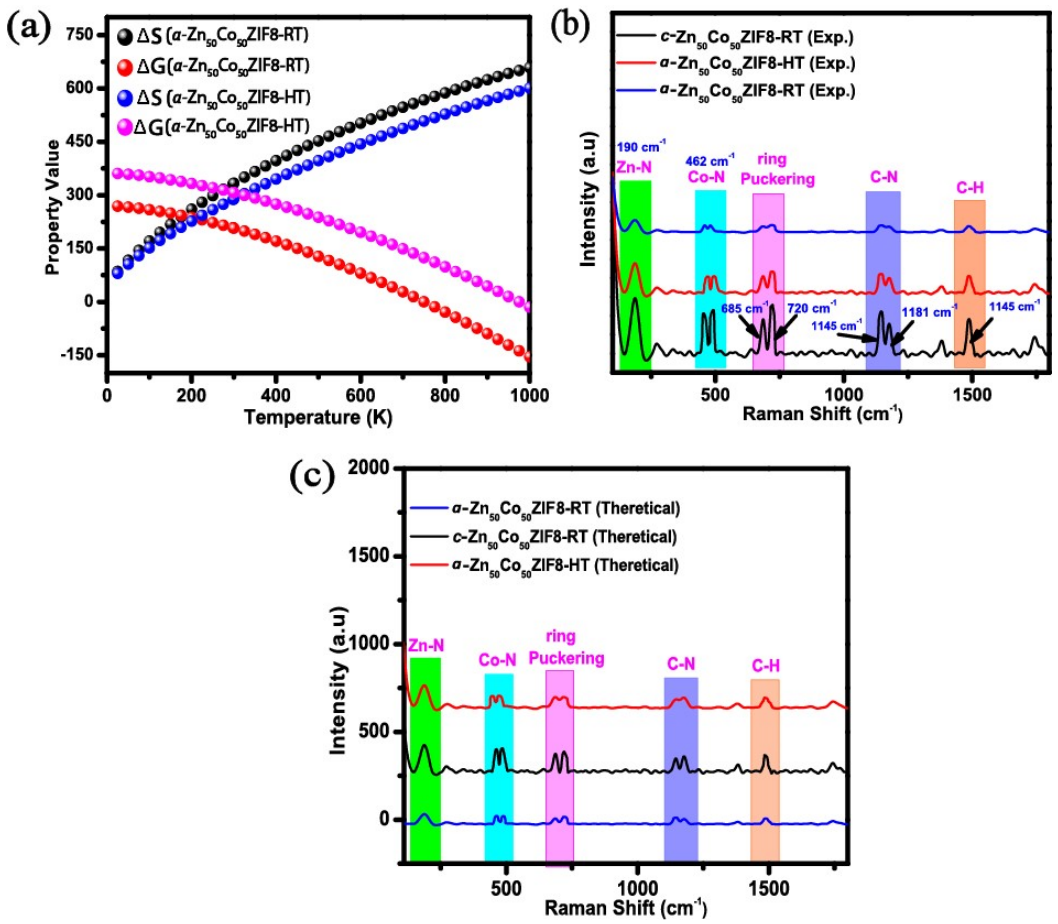

Figure S22: Theoretical thermodynamic study (ΔS and ΔG) of (a) *a*-$Zn_{50}Co_{50}$ZIF8-RT (black), *a*-$Zn_{50}Co_{50}$ZIF8-RT (red), *a*-$Zn_{50}Co_{50}$ZIF8-HT (blue) and *a*-$Zn_{50}Co_{50}$ZIF8-HT (pink). Experimental Raman spectra of (b) *c*-$Zn_{50}Co_{50}$ZIF8-RT (black), *a*-$Zn_{50}Co_{50}$ZIF8-HT (red) and *a*-$Zn_{50}Co_{50}$ZIF8-RT (blue). (c) Theretical Raman spectra of *c*-$Zn_{50}Co_{50}$ZIF8-RT (black), *a*-$Zn_{50}Co_{50}$ZIF8-HT (red) and *a*-$Zn_{50}Co_{50}$ZIF8-RT (blue).

Section S5: Electrochemical measurements

The electrochemical experiments were performed in 1 M KOH. 5 mg catalyst was dispersed in a mixture solution (250 μL water, 245 μL ethanol and 5 μL Nafion) to prepare catalyst ink. Afterward, 5 μL ink was loaded on the glassy carbon electrode (GCE), containing 0.05 mg of catalyst on a 0.07 cm^2 area of GCE. All the electrochemical experiments were carried out using CHI 620E electrochemical workstation with a three-electrode system where Hg/HgO and graphite rod were used as reference and counter electrodes. The GCE electrode coated with a catalyst was used as a working electrode. To activate and stabilize the electrode, 50 cyclic voltammetry (CV) cycles were performed at the scan rate of 100 mV s^{-1}. The OER overpotential was obtained by performing linear sweep voltammetry (LSV) curves at the scan rate of 2 mV s^{-1}. All the potential values were converted by the reversible hydrogen electrode (RHE) scale by the given equation.

$$E_{RHE} = E_{Hg/HgO} + 0.1 + 0.059 \times pH$$

Where $E_{Hg/HgO}$ is the potential obtained against Hg/HgO electrode, 0.1 is the standard potential of Hg/HgO electrode.

The equation to calculate Tafel slope are given below;

$\eta = a + b^* \log j$,

where η, b and j are overpotential, Tafel slope and current density, respectively.

Calculation of turnover frequency

The turnover frequency (TOF) for HER can be calculated using the equation below:

$$TOF = J/(2 \square x F)$$

where J is the current density (A cm^{-2}) at specific potential (200 mV), x is the number of moles of catalyst loaded on the working electrode, F is the Faradays constant and the term ½ is used because HER is a 2 electron reaction.

The TOF can be calculated for OER by the equation given below:

$$TOF = J/(4xF)$$

where the term ¼ is used because of the involvement of 4 electrons in OER.[2]

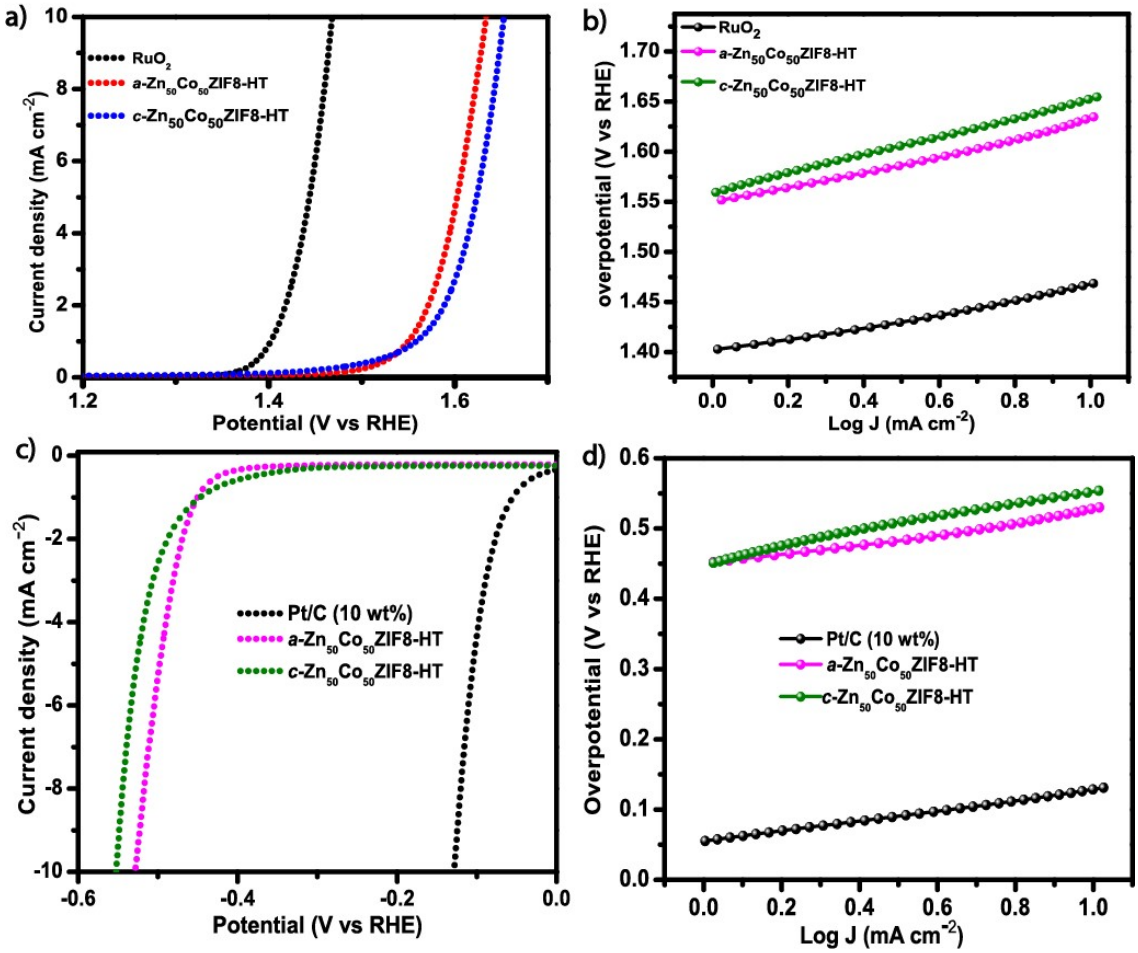

Figure 23: Electrochemical performance of the *a*-$Zn_{50}Co_{50}$ZIF8-HT catalysts: a) linear sweep voltammetry (LSV) curves and b) Tafel slopes for oxygen evolution reactions (OER). c) LSV curves and (d)Tafel slopes for hydrogen evolution reactions (HER) of all catalysts at a current density of 10 mA cm^{-2}.

5.1 TOF and C_{dl} value

The turnover frequency (TOF) has been calculated for all the synthesized MOF materials for HER and OER at a fixed overpotential of 400 mV. *a*-$Zn_{50}Co_{50}$ZIF8-RT exhibits a higher TOF value of 3.6 x 10^{-3} s^{-1} compared to *c*-$Zn_{50}Co_{50}$ZIF8-RT (0.6 x 10^{-3} s^{-1}), *a*-$Zn_{50}Co_{50}$ZIF8-HT (0.9 x 10^{-3} s^{-1}), *c*-$Zn_{50}Co_{50}$ZIF8-HT (0.6 x 10^{-3} s^{-1}), *p*Co-ZIF8-RT (0.4 x 10^{-3} s^{-1}) and *p*Zn-ZIF8-RT (0.1 x 10^{-3} s^{-1}) for HER and similarly the TOF values were calculated for OER which shows that *a*-

$Zn_{50}Co_{50}$ZIF8-RT have a higher TOF value of 35.2 x 10^{-3} s^{-1} compared to *c*-$Zn_{50}Co_{50}$ZIF8-RT (27.6 x 10^{-3} s^{-1}), *a*-$Zn_{50}Co_{50}$ZIF8-HT (7.7 x 10^{-3} s^{-1}), *c*-$Zn_{50}Co_{50}$ZIF8-HT (4.8 x 10^{-3} s^{-1}), *p*Co-ZIF8-RT (10.2 x 10^{-3} s^{-1}) and *p*Zn-ZIF8-RT (0.4 x 10^{-3} s^{-1}). Further, these result are compared in Figure 24(a). The C_{dl} values are calculated and compared in Figure 24(b).

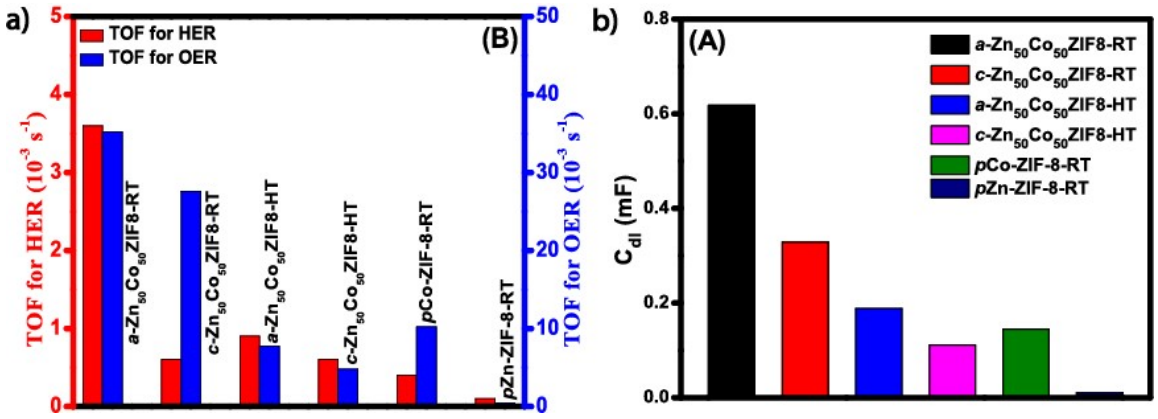

Figure S24: Bar graph of all synthesized material (a) TOF values calculated for HER and OER and (b) C_{dl} values.

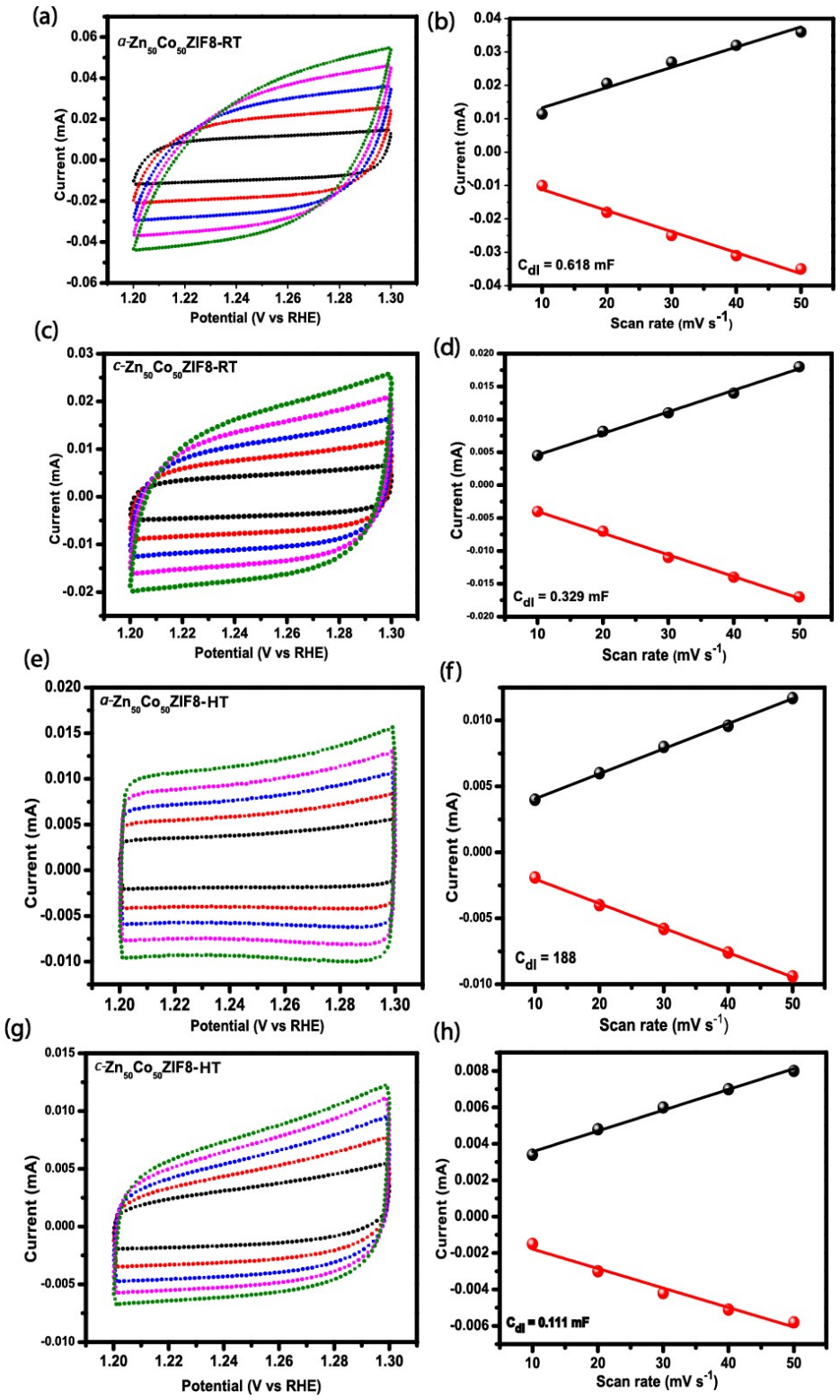

Figure S25: Cyclic voltammetry (CV) cycles at different scan rate from 10 to 50 mV s^{-1} in 1M KOH for (a) *a*-$Zn_{50}Co_{50}$ZIF8-RT, (c) *c*-$Zn_{50}Co_{50}$ZIF8-RT, *(e)* *a*-$Zn_{50}Co_{50}$ZIF8-HT *(g)* *c*-

$Zn_{50}Co_{50}$ZIF8-HT. Corresponding anodic and cathodic current slope from the CV curves of (b) *a*$Zn_{50}Co_{50}$ZIF8-RT, *(d) c*-$Zn_{50}Co_{50}$ZIF8-RT, *(f) a*-$Zn_{50}Co_{50}$ZIF8-HT and (h) *c*-$Zn_{50}Co_{50}$ZIF8-HT.

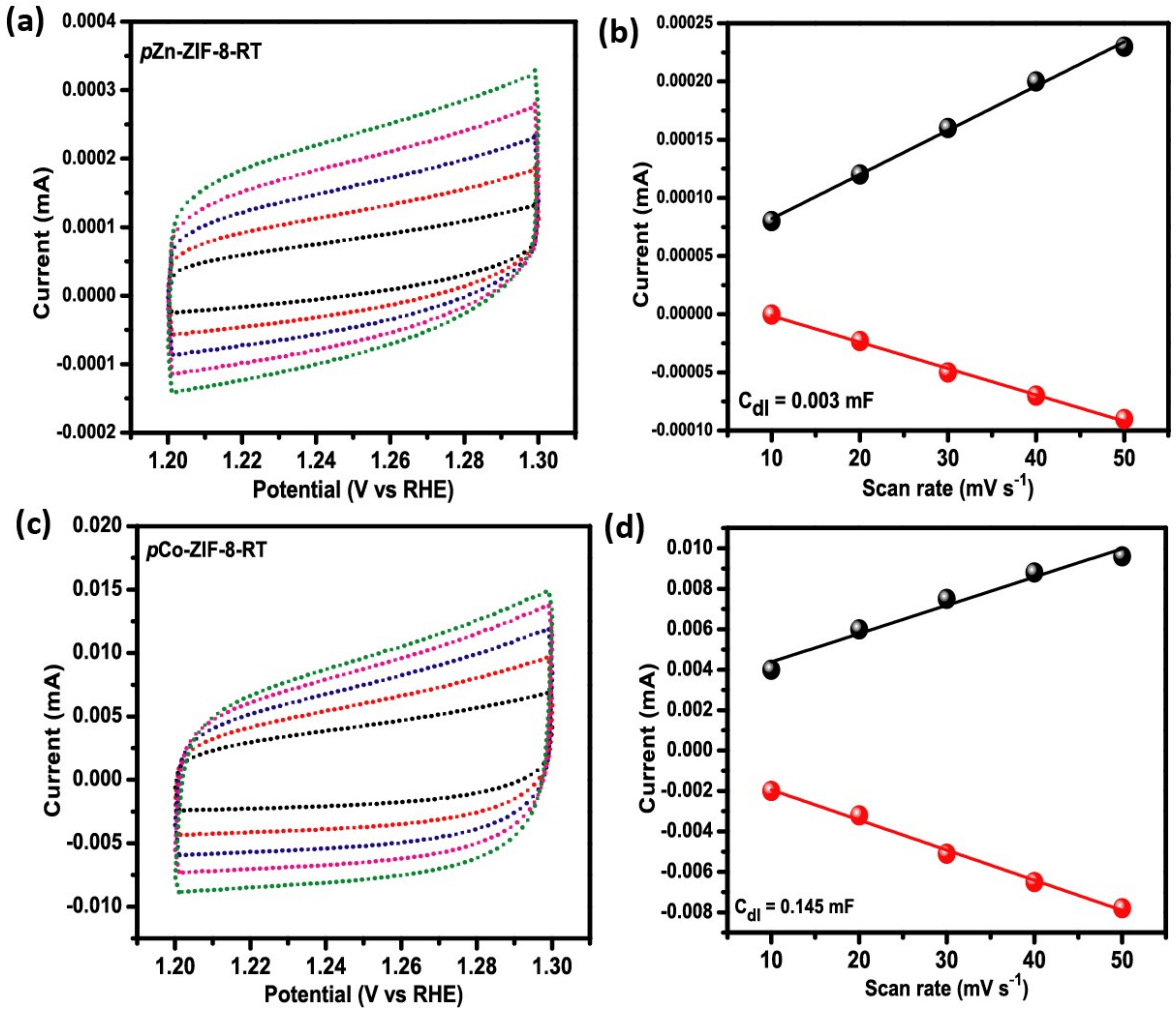

Figure S26: Cyclic voltametry (CV) cycles at different scan rate from 10 to 50 mV s^{-1} in 1M KOH for (a) *p*Zn-ZIF-8-RT and (c) *p*Co_ZIF-8-RT. Corresponding anodic and cathodic current slope from the CV curves of (b) *p*Zn-ZIF-8-RT and (d) *p*Co_ZIF-8-RT.

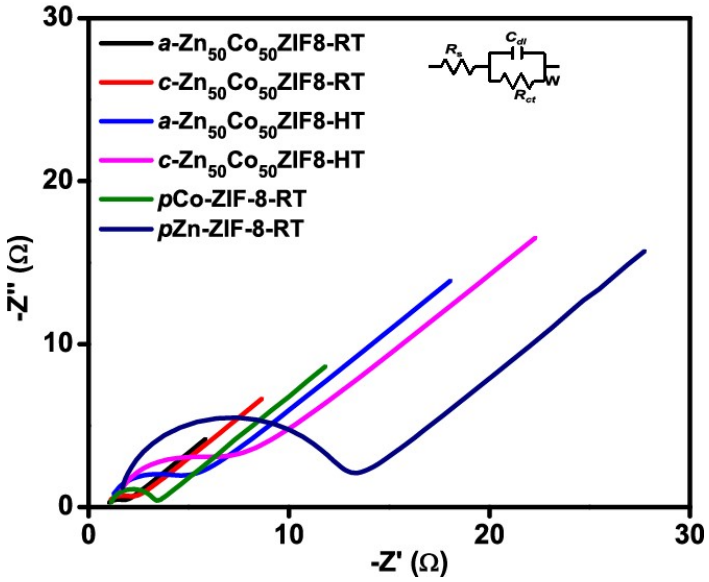

Figure S27: Nyquist plots of all the synthesized materials (Inset) equivalent circuit.

5.2 Overall Water Splitting

In order to demonstrate the overall water splitting, a two-electrode setup was prepared, where *a*-$Zn_{50}Co_{50}$ZIF8-RT as anodic and cathodic material. Similarly, for comparison, *c*-$Zn_{50}Co_{50}$ZIF8-RT was also utilized as bifunctional electrocatalyst for overall water splitting in 1 sM KOH.

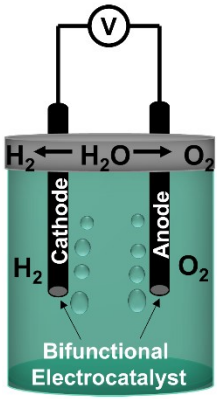

Figure S28. Schematic of a two-electrode system constructed for overall water splitting.

Table S2. Electrocatalytic performance of different synthesized electrocatalysts towards both OER and HER activity:

Electrocatalysts	OER		HER		C_{dl} (mF)	ECAS (cm^2)	R_{ct} (Ω)
	Overpotential (mV) at (η^{10})	Tafel Slope (mV dec^{-1})	Overpotential (mV) at (η^{10})	Tafel Slope (mV dec^{-1})			
a-$Zn_{50}Co_{50}$ZIF8-RT	301	59	437	57.8	0.618	15.45	0.77
c-$Zn_{50}Co_{50}$ZIF8-RT	330	80	491	65.6	0.329	8.22	1.16
a-$Zn_{50}Co_{50}$ZIF8-HT	400	82.4	528	77	0.188	4.70	3.32
c-$Zn_{50}Co_{50}$ZIF8-HT	423	91.6	551	102	0.111	2.77	4.81
*p*Co-ZIF-8-RT	384	94.1	582	96.7	0.145	3.62	2.13
*p*Zn-ZIF-8-RT	-	-	-	-	0.003	0.07	10.64

5.3 Chronoamperometry Study

Electrochemical studies were carried out using a glassy carbon electrode (GCE), more bubbles were generated while on the surface of the GCE applying a higher current density, which makes noise in the electrochemical data. Hence, the chronoamperometry has been reported at 10 mA cm^{-2} (Figure S29). However, to perform the overall water splitting at a higher current density, *a*-$Zn_{50}Co_{50}$ZIF8-RT was coated on carbon cloth (1 x 1 cm^2) using the drop casting method. The chronoamperometry was performed at a fixed potential at 50 mA cm^{-2} current density, as shown in Figure S30. The chronoamperometric curve shows a stable current response at a fixed potential for 48 h. Thus, the results obtained suggest the excellent long-term stability of *a*-$Zn_{50}Co_{50}$ZIF8-RT.

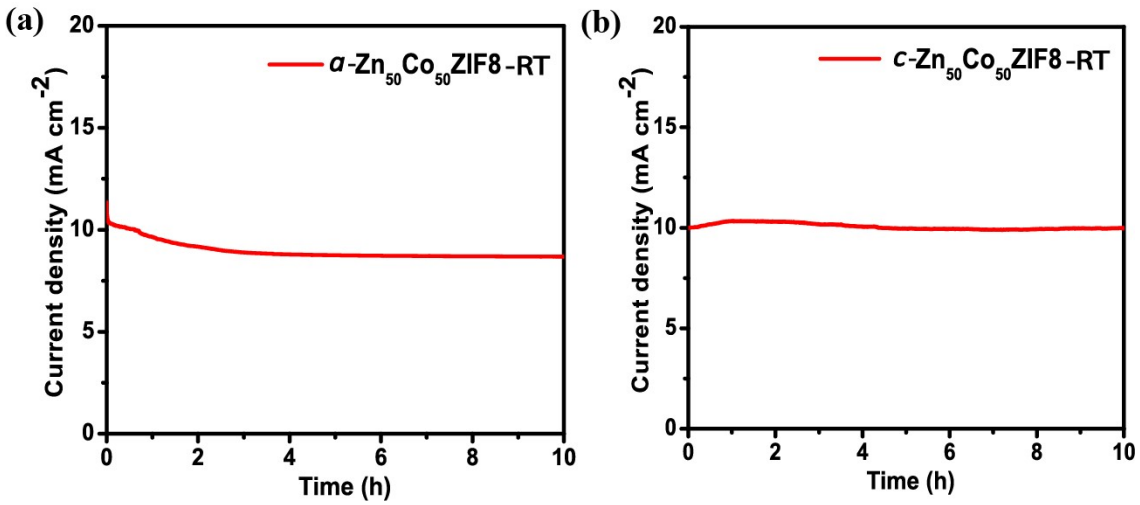

Figure S29: (a, b) Chronoamperometry curve of *a*-$Zn_{50}Co_{50}$ZIF8-RT and *c*-$Zn_{50}Co_{50}$ZIF8-RT at the current density of 10 mA cm^{-2}.

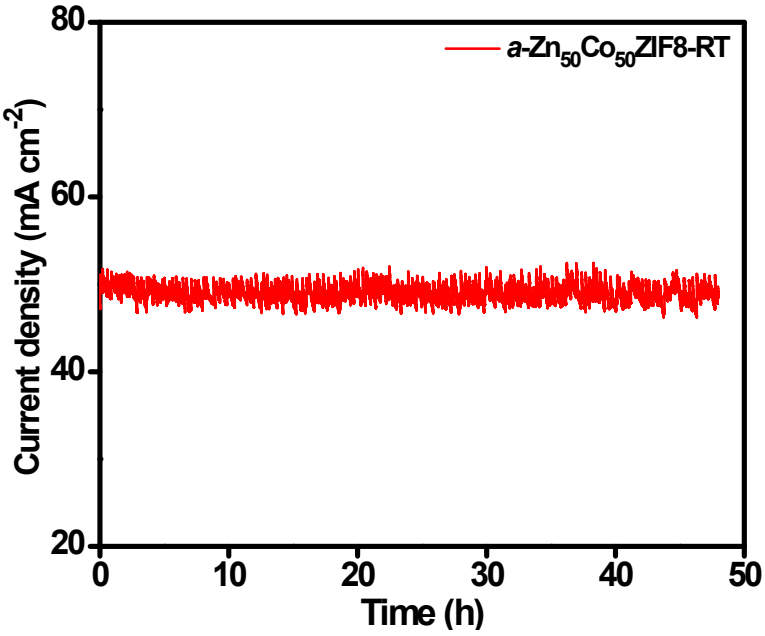

Figure S30: Chronoamperometry curve of *a*-$Zn_{50}Co_{50}$ZIF8-RT at 50 mA cm^{-2} in 1 M KOH.

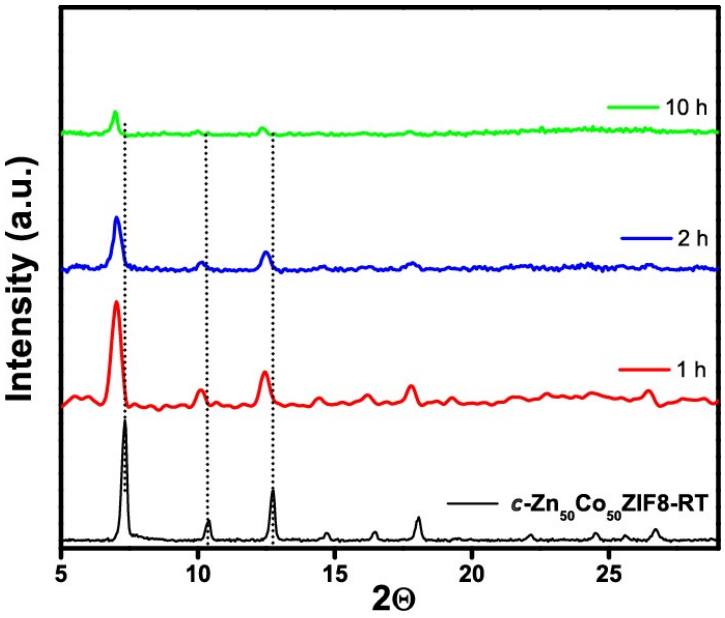

Figure S31: PXRD measurements of *c*-$Zn_{50}Co_{50}$ZIF8-RT (black) performed after OER stability test in 1M KOH (at 25 °C) for 1 h (red), 2 h (blue) and 10 h (green). Pxrd plot indicate that the structure is stable upto 1 h, 2 h and 10 h also.

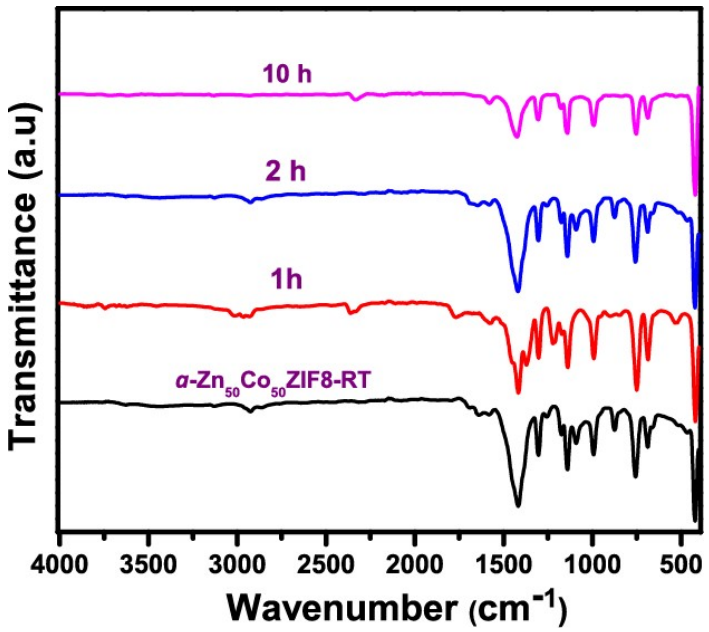

Figure S32: FT-IR measurement of *a*-$Zn_{50}Co_{50}$ZIF8-RT (black) performed after OER stability test in 1M KOH (at 25 °C) for 1 h (red), 2 h (blue) and 10 h (pink). FT-IR indicate that the structure is stable upto 1 h, 2 h and 10 h also.

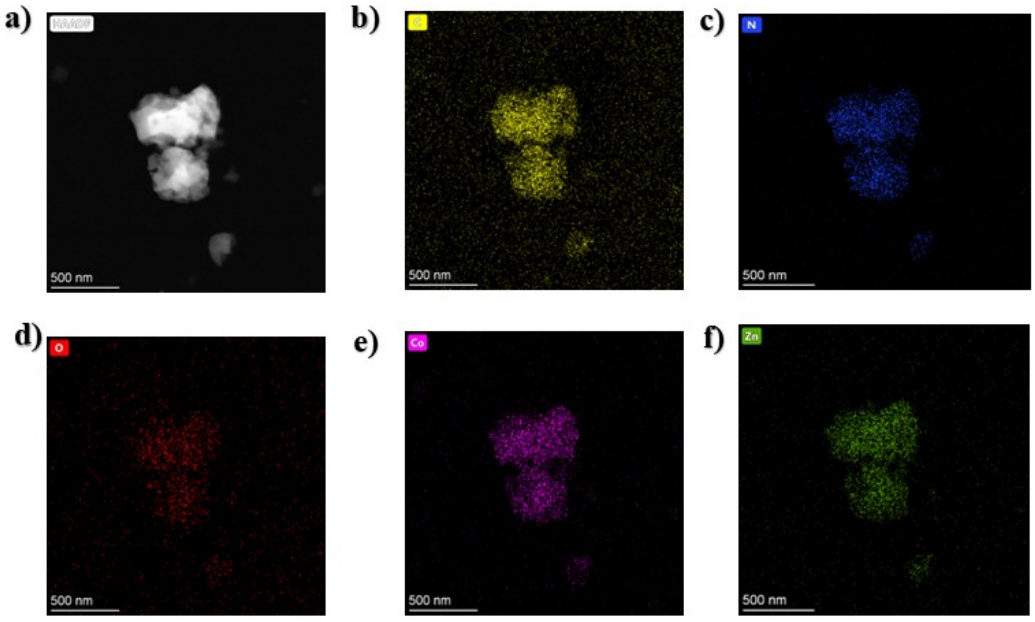

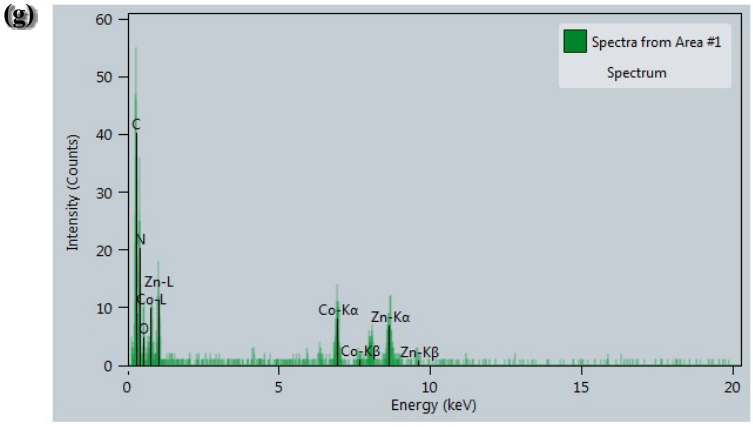

Z	Element	Family	Atomic Fraction (%)	Atomic Error (%)	Mass Fraction (%)	Mass Error (%)	Fit error (%)
6	C	K	63.99	5.73	44.21	2.45	2.27
7	N	K	22.18	4.89	17.87	3.73	3.34
8	O	K	4.33	1	3.99	0.87	7.46
27	Co	K	4.85	0.78	16.43	2.38	2.42
30	Zn	K	4.65	0.75	17.5	2.54	2.64

Figure S33: STEM elemental mapping of *a*-$Zn_{50}Co_{50}$ZIF8-RT before catalysis (a) STEM images of the particle selected for elemental mapping (b) C distribution (c) N distribution (d) O distribution (e) Co distribution (f) Zn distribution and (g) EDAX spectrum of elemental mapping.

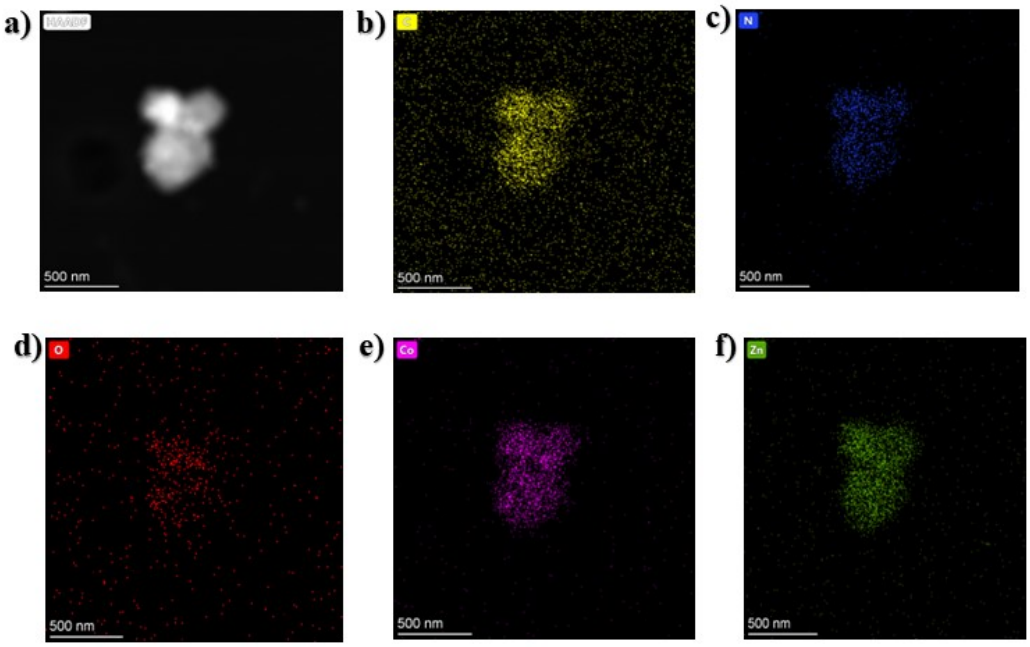

(g)

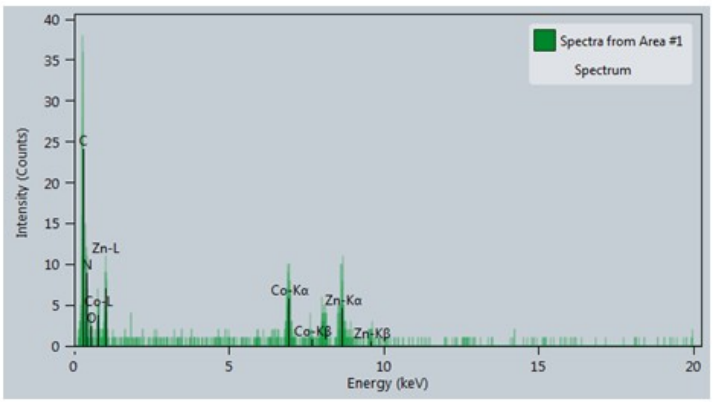

Z	Element	Family	Atomic Fraction (%)	Atomic Error (%)	Mass Fraction (%)	Mass Error (%)	Fit error (%)
6	C	K	67.51	6.37	44.22	2.85	3.94
7	N	K	17.15	3.83	13.1	2.78	5.04
8	O	K	3.67	0.95	3.2	0.8	13.99
27	Co	K	6.14	1	19.72	2.9	3.5
30	Zn	K	5.54	0.91	19.75	2.94	4.24

Figure S34: STEM elemental mapping of *a*-$Zn_{50}Co_{50}$ZIF8-RT after catalysis (a) STEM images of the particle selected for elemental mapping (b) C distribution (c) N distribution (d) O distribution (e) Co distribution (f) Zn distribution and (g) EDAX spectrum of elemental mapping.

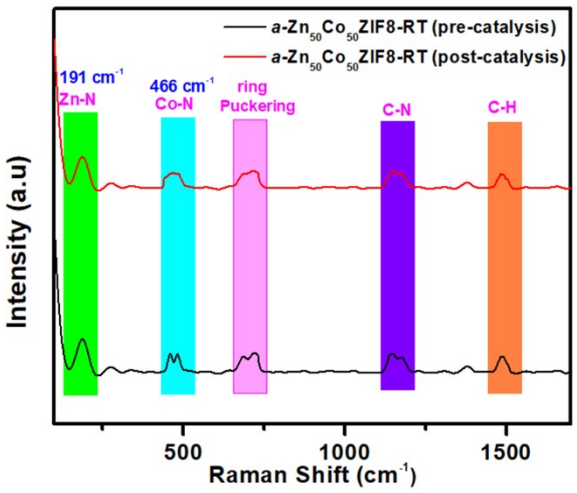

Figure S35: Experimental Raman spectra of (a) *a*-$Zn_{50}Co_{50}$ZIF8-RT (black) before and after (red) catalysis.

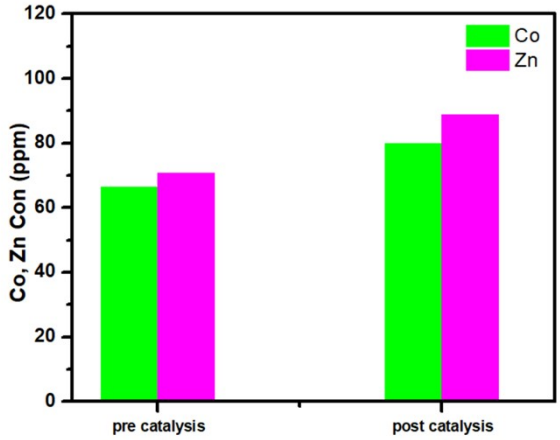

Samples	Co	Zn
	ppm	ppm
***a*-$Zn_{50}Co_{50}$ZIF8-RT (pre catalysis)**	**66.52**	**70.72**
***a*-$Zn_{50}Co_{50}$ZIF8-RT (post catalysis)**	**80.1**	**88.8**

Figure S36: ICP–MS analysis showing the amounts of Co and Zn during pre- and post catalytic study.

Table S3: The comparison of the electrocatalytic HER performance of recently reported MOFs.

Catalysts	Overpotential (mV) at 10 mA cm^{-2}	Tafel slope (mV dec^{-1})	Electrolyte	Substrate	References
Co-BTC	437	115	1.0 M KOH	CC	[3]
C–NiCu–BDC MOF	400	-	1.0 M KOH	CC	[4]
CoDBP/(CNTs)	650	178	0.026 M TFA	GCE	[5]
3D Co/Ni-MOFs	357	107	0.5 M H_2SO_4	GCE	[6]
THTA–Co/G	283	71	0.5 M H_2SO_4	GCE	[7]
Co-MOF	400	65	0.5 M H_2SO_4	GCE	[8]
***a*-$Zn_{50}Co_{50}$ZIF8-RT**	**301**	**59**	**1.0 M KOH**	**GCE**	**This work**

Table S4: The comparison of the electrocatalytic OER performance of recently reported MOFs.

Catalysts	Overpotential (mV) at 10 mA cm^{-2}	Tafel slope (mV dec^{-1})	Electrolyte	Substrate	References
$Co_2(\mu\text{-}OH)_2$(bbta)	421	95	1.0 M KOH	CC	[9]
Co-ZIF	510@1 mA cm^{-2}	193	1.0 M KOH	FTO	[10]
Co-WOC-1	390@1 mA cm^{-2}	128	0.1 M KOH	GCE	[11]
Co_3O_4/C	520	142	0.1 M KOH	Cu Foil	[12]
Co_2-tzpa	396	88	0.1 M KOH	GCE	[13]
MIL-126(FeCo)-700	560	-	0.1 M KOH	GCE	[14]
***a*-$Zn_{50}Co_{50}$ZIF8-RT**	**437**	**57.8**	**1.0 M KOH**	**GCE**	**This work**

Table S5: Cell potential comparison of various MOF-based electrocatalysts for overall water splitting.

Catalyst	Cell Potential (V at 10 mA cm^{-2})	Substrate	Electrolyte	Reference
Co–BTC MOF	2.03	Carbon cloth	1 M KOH	[3]
C–NiCu–BDC MOF	2.05	Carbon cloth	1 M KOH	[4]
***a*-$Zn_{50}Co_{50}$ZIF8-RT**	**1.97**	**Glassy carbon**	**1 M KOH**	**This work**

References:

1. (*a*) Y. Pan, Y. Liu, G. Zeng, L. Zhao and Z. Lai, *Chem. Commun.*, 2011, **47**, 2071–2073; (*b*) K. S. Park, Z. Ni, A. P. Côté, J. Y. Choi, R. Huang, F. J. Uribe-Romo, H. K. Chae, M. O'Keeffe and O. M. Yaghi, *Proc. Natl. Acad. Sci. U. S. A,* 2006, **103**, 10186–10191**.**

2. A. Kareem, K. Theyagarajan, K. Thenmozhi, S. Pitchaimuthu and S. Senthilkumar, *Adv. Sustainable Syst*., 2025, **9**, e01270.

3. S. N. Shreyanka, J. Theerthagiri, S. J. Lee, Y. Yu and M. Y. Choi, *Chem. Eng. J,* 2022, **446**, 1-40.

4. L. Jia, P. Wagner and J. Chen, *Inorganics,* 2022, **10**, 53.

5. D. Micheroni, G. Lan and W. Lin, *J. Am. Chem. Soc*., 2018, **140**, 15591-15595.

6. X. Wang, J.-Y. Luo, J.-W. Tian, D.-D. Huang, Y.-P. Wu, S. Li and D.-S. Li, *Inorg. Chem. Commun*., 2018, **98**, 141-144.

7. R. Dong, Z. Zheng, D. Tranca, J. Zhang, N. Chandrasekhar Reddy, S. Liu, X. Zhuang, G. Seifert and X. Feng, *Chem.-Eur. J.,* 2016, **23**, 2255-2260.

8. V. Khrizanforova, R. Shekurov, V. Miluykov, M. Khrizanforov, V. Bon, S. Kaskel, A. Gubaidullin, O. Sinyashin and Y. Budnikova, *Dalton Trans*., 2020, **49**, 2794-2802.

9. X.-F. Lu, P.-Q. Liao, J.-W. Wang, J.-X. Wu, X.-W. Chen, C.-T. He, J.-P. Zhang, G.-R. Li and X.-M. Chen, *J. Am. Chem. Soc*., 2016, **138**, 8336-8339.

10. S. Wang, Y. Hou, S. Lin and X. Wang, *Nanoscale,* 2014, **6**, 9930-9934.

11. P. Manna, J. Debgupta, S. Bose and S. Das, *Angew. Chem. Int. Ed*., 2016, **55**, 2425-2430

12. T.Y. Ma, S. Dai, M. Jaroniec and S. Z. Qiao, *J. Am. Chem. Soc*., 2014, **136**, 13925-13931.

13. N. Liu, Q. Zhang and J. Guan, *ChemComm*., 2021, **57**, 5016-5019.

14. Z. Lionet, S. Nishijima, T.-H. Kim, Y. Horiuchi, S.W. Lee and M. Matsuoka, *Dalton Trans*.,

2019, **48**, 13953-13959.